# Northern North Atlantic climate variability controls on ocean carbon sinks in EC-Earth3-CC

Anna Pedersen[1,2], Carolin R. Löscher[1], Steffen M. Olsen[2]

[1]Nordcee, University of Southern Denmark, Odense, 5230, Denmark

5  [2]Danish Meteorological Institute, National Centre for Climate Research, Copenhagen, 2100, Denmark

*Correspondence to*: Anna Pedersen (annapedersen@biology.sdu.dk)

**Abstract**

The northern North Atlantic is an important net sink of atmospheric $CO_2$, though atmosphere–ocean $CO_2$ fluxes exhibit substantial variability across different timescales. The underlying drivers of this variability remain poorly understood across

10  both temporal and regional scales. Here, we investigate interannual to decadal $CO_2$ flux variability in the northern North Atlantic using historical simulations from the EC-Earth3-CC model. We assess the role of key dynamical and physical processes in shaping $CO_2$ flux variability across five regions: the Nordic Seas, eastern Nordic Seas, the eastern and western subpolar North Atlantic, and the full North Atlantic. Our analysis reveals that physical parameters—including sea ice concentration (SIC), sea surface temperature (SST), sea surface salinity (SSS), and wind stress—along with dynamical

15  processes related to ocean mixing and circulation, play a central role in regulating $CO_2$ flux variability. Using regression analysis, we demonstrate that these drivers exert regionally and temporally varying influences, with our models achieving high $R^2$ values indicating a strong degree of explanation for $CO_2$ flux variability. The regression models capture interannual variability more effectively than decadal variability, highlighting the dominant role of short-term fluctuations in shaping $CO_2$ flux dynamics. Overall, our results demonstrate that the predictors of $CO_2$ flux variability are both spatially and temporally

20  dependent. We find that $CO_2$ flux variability cannot be fully explained by simple linear correlations with individual predictors but instead arises from complex interactions among multiple physical and dynamical processes. Notably, $CO_2$ flux variability is particularly sensitive to changes in certain predictors, such as wind stress, consistent with expectations based on the gas transfer equation used to compute atmosphere–ocean $CO_2$ fluxes.

## 1. Introduction

The northern North Atlantic is a net sink of atmospheric carbon dioxide ($CO_2$; Fig. 1a; Gruber et al., 2002; Takahashi et al., 2009, Yu et al., 2019). This sink is primarily driven by the combined effects of the solubility pump and the biological carbon pump. The solubility pump enhances $CO_2$ uptake through two key mechanisms: (1) the cooling of northward-flowing warm waters, which increases $CO_2$ solubility at the surface, and (2) the formation of dense, cold deep water at high latitudes, which transports $CO_2$-enriched surface waters into the ocean interior as part of the Atlantic thermohaline circulation (Volk et al., 1985). The biological carbon pump further contributes by fixating carbon through photosynthesis and primary production (PP), exporting organic carbon to the deep ocean, and maintaining a net sink of atmospheric $CO_2$ in the region (Sigman and Boyle, 2000; Boyd and Trull, 2007; Sanders et al., 2014). Currently, the North Atlantic absorbs a significant fraction of anthropogenic $CO_2$ emissions, accounting for approximately one-quarter to one-third of global anthropogenic carbon uptake (Khatiwala et al., 2009; Sabine et al., 2004; Breeden and McKinley, 2016; Le Quéré et al., 2018; Gruber et al., 2019). In contrast, the global ocean uptake is around 25% of annual emissions due to outgassing in some ocean regions (Fig. 1; Landschützer et al., 2016; Mikaloff Fletcher et al., 2006; Khatiwala et al., 2013; Le Quéré et al., 2015; Friedlingstein et al., 2023; Gruber et al., 2023; Terhaar et al., 2022).

Beyond these large-scale mechanisms, the strength of the North Atlantic $CO_2$ sink varies seasonally and interannually, influenced by ocean-atmosphere interactions. Biological productivity peaks in spring and summer, enhancing $CO_2$ drawdown, while wintertime cooling promotes solubility-driven uptake (Ardyna and Arrigo 2020). These processes are modulated by climate variability, particularly the North Atlantic Oscillation (NAO) and the Atlantic Multidecadal Oscillation (AMO; Leseurre et al., 2020). Additionally, physical processes such as warming and cooling cycles, deep convection, and changes in ocean circulation and water masses in the subpolar gyre (SPG) play a crucial role in regulating air-sea $CO_2$ fluxes. These physical drivers are closely linked to NAO and AMO variability, further influencing regional $CO_2$ uptake dynamics (Chafik et al., 2019; Desbruyëres et al., 2015). Breeden and McKinley (2016) show that a North Atlantic basin-average sea surface temperature (SST) is associated with the leading mode of surface ocean $pCO_2$ variability based on an analysis of a regional model. The SST signal is affected by an upward trend due to greenhouse gas emissions and a signal of internal variability due to the AMO (Kerr, 2000). Furthermore, they establish that physical (in contrast to the chemical) variability is the dominant driver of variability in the North Atlantic surface ocean carbon cycle. During a positive phase of the AMO an increase in sea (surface) temperature increases $pCO_2$ due to the reduction in solubility (an increase in the fugacity of $CO_2$, $fCO_2$) resulting in a reduced flux of $CO_2$ into the ocean (also seen in Breeden and McKinley (2016)). Studies show that on a decadal scale the AMO and $fCO_2$ variability in the SPG correlates (Breeden and McKinley, 2016; Landschutzer et al., 2019; Leseurre et al., 2020): as the AMO enters a positive (warm) phase, reduced mixing (a shallowing of the mixed layer depth) results in a reduced supply of dissolved inorganic carbon (DIC) from the subsurface layers, a process that dominates the effect of warming on the solubility and $fCO_2$. The surface ocean's ability to absorb anthropogenic carbon is primarily regulated by carbonate chemistry, particularly alkalinity (Broecker et al., 1979; Terhaar et al., 2022).

While increasing anthropogenic carbon generally enhances ocean carbon uptake, this relationship is moderated by rising global temperatures, which reduce solubility, and further influenced by decadal variability and long-term trends. However, the underlying drivers of these trends remain poorly understood (Terhaar, 2024).

The subpolar North Atlantic has experienced significant interannual to decadal variability in ventilation depth during the industrial period (Polyakov 2005; Holliday et al., 2020; Zou et al., 2023, Thomas and Zhang 2022). Recent studies highlight pronounced ocean variability in the Subpolar Gyre region, including the formation of cold and fresh anomalies. Holliday et al. (2020) documented a substantial freshening event in the eastern subpolar North Atlantic, the most significant in 120 years, attributed to wind-driven circulation changes that redistributed freshwater within the region. Similarly, Zou et al. (2023) identified two sources of deep ocean variability in the central Labrador Sea, furthering our understanding of long-term property anomalies in the western subpolar North Atlantic. These findings underscore the SPG's dynamic nature and its sensitivity to both atmospheric and oceanic forcing. The SPG, a counterclockwise gyre system, plays a crucial role in modulating ocean circulation by introducing saline Atlantic Water into the northern North Atlantic. The North Atlantic Current follows the southern and eastern boundaries of the SPG, transporting warm, saline water from the Gulf Stream into the northern North Atlantic and eventually the Arctic (Holliday et al., 2020; Daniault et al., 2016; Hátún et al., 2017). At the same time, freshwater from the Arctic is supplied to the SPG, contributing to temporal variability in ocean properties. These processes are key regulators of the AMOC (Holliday et al., 2020; Hátún et al., 2005, 2017). The strength of the SPG circulation strongly influences both physical and biological processes in the northern North Atlantic. A weak (strong) SPG leads to a shallowing (deepening) of sea surface height (SSH) and, consequently, a shallowing (deepening) of the mixed layer depth (MLD). Additionally, a weak SPG contracts westward, allowing nutrient-poor subtropical waters to penetrate northward, warming the gyre and reducing primary production. In contrast, a strong SPG expands eastward, accumulates Arctic fresh and nutrient-rich water within the gyre system, increasing PP and solubility, and limits the intrusion of warm, saline Atlantic Water into the region (Häkkinen et al., 2013; Hátún et al., 2005, 2017; Foukal et al., 2017). Importantly, variations in SSS serve as an indicator of these gyre dynamics and ocean mixing processes, making it a valuable indirect predictor of $CO_2$ flux variability. Changes in salinity reflect shifts in water mass distribution, stratification, and ventilation, all of which influence air-sea gas exchange. Therefore, monitoring SSS variability can provide critical insights into the mechanisms driving $CO_2$ flux variability in the North Atlantic (Thomas and Zhang, 2022).

Understanding the vulnerability of the ocean carbon sink to future climatic changes is the motivator for our analysis. Expected future decline in the strength of the Atlantic Meridional Ocean Circulation (AMOC; Fox-Kemper et al., 2023) will likely result in a declining ocean $CO_2$ uptake due to less transport of $CO_2$ enriched surface waters into the deep ocean. Projections indicate a reduced $CO_2$ uptake/sink in the global oceans correlating with a gradual reduction of the strength of the AMOC (McKinley et al., 2023; Liu et al., 2023). A slowing AMOC impacts ocean biology and solubility carbon pumps: CMIP5 analysis projects a weakening of the biological pump from surface waters with the largest decreases in effective $CO_2$ uptake under the strongest warming scenarios (Bopp et al., 2013; Fu et al., 2016; Laufkötter et al., 2016; Liu et al., 2023). This is in part explained by ocean warming, which result in a decline in PP, also contributing to a decrease in

ocean $CO_2$ uptake in some regions (Kwiatokowski et al., 2020), however ocean warming and climate change also leads to sea ice decline, which results in increased PP regionally (Vancoppenolle et al., 2013). The projected climate driven impacts on the AMOC are yet not seen in the strength of regional components of the AMOC in the northern North Atlantic (Østerhus et al., 2019; Lozier et al., 2019; Orvik et al., 2022). Also, over the last two decades the estimated AMOC strength at 26°N is dominated by interannual to decadal variability with a marginal significant negative trend (Volkov et al., 2024). These findings underscore how variability in North Atlantic ocean and climate conditions, including fluctuations in AMOC strength, can modulate both the magnitude and regional distribution of oceanic $CO_2$ sinks.

We aim to understand the sensitivity and drivers of the atmosphere–ocean $CO_2$ flux in an ESM system on interannual and decadal timescales. Through our analysis we establish which predictors can explain the $CO_2$ flux variability in the five regions of the northern North Atlantic. We define regression models based on physical and dynamic predictors, to explore how well we can predict and understand future $CO_2$ flux variability.

## 1.1 Approach

The aim of this work is to understand how simulated interannual to decadal variability can help build confidence in future changes and a better understanding of uncertainties related to ocean processes and variability. We analyse ensemble data from 10 historical simulations with the EC-Earth3-CC global climate model with interactive ocean biogeochemical cycling. To assess the drivers of the interannual and decadal $CO_2$ flux variability in the northern North Atlantic we initially establish an overview of the relationship between the $CO_2$ flux variability and parameters that could potentially drive this variability across the northern north Atlantic and in defined sub regions (Fig. 1b).

Firstly, we use the gas transfer equations to check if we can reproduce the simulated $CO_2$ flux variability in the different regions from archived model data for the individual ocean region. Based on the gas transfer equation (Eq. 1-3) we expect SST, sea surface salinity (SSS), $\Delta pCO_2$, wind and sea ice concentration (SIC) to be controlling physical parameters driving the simulated $CO_2$ flux variability. We additionally explore the relation of integral between $CO_2$ flux variability and parameters representing ocean dynamics or processes by including parameters such as mixed layer depth (MLD) and sea surface height (SSH), which are not direct drivers of atmosphere–ocean gas exchange. For each region, we integrate the $CO_2$ flux and define high and low $CO_2$ flux years for short and long timescales. We construct ensemble mean composite 2D maps of the $CO_2$ flux by subtracting the low flux years from the high flux years and by combining all ensemble members. We use the high and low flux years defined for the $CO_2$ flux to also construct composite maps of other key physical parameters.

Secondly, informed by the composite maps and identified controls of the $CO_2$ flux variabillity, we define ten indexes that can be correlated with the $CO_2$ flux timeseries. The indexes are based on the parameters contributing to the gas exchange equations (Eq. 1-3) SST (AMO), SSS, wind and SIC, climatic modes of variability such as NAO, the ocean circulation strength (SSH index representing gyre circulation strength), MLD and AMOC. The specific definition of the different indexes and why we have chosen them is described in section 3. We have chosen to exclude $\Delta pCO_2$ and other

biogeochemical parameters, to focus our analysis on the physical processes and dynamical parameters affecting $CO_2$ flux variability.

Lastly, in order to understand how much of the $CO_2$ flux variability that can be explained and described by physical variables and indexes alone, we set up simple linear multivariable regression models for each region and discuss differences in explained variability across interannual and decadal timescales.

## 1.2 EC-Earth3-CC

EC-Earth3-CC is the carbon cycle (CC) version of the EC-Earth3. EC-Earth3 is an Earth system model, developed by the EC-Earth consortium (https://ec-earth.org), and contributes to the Coupled Model Intercomparison Project (CMIP). EC-Earth3 comprises several model components describing atmosphere, ocean, sea ice, land surface, dynamic vegetation, atmospheric chemical composition, ocean biogeochemistry and the Greenland Ice Sheet. EC-Earth3 (Döscher et al., 2022) consists of the atmosphere model IFS, land surface module HTESSEL and the ocean model NEMO3.6 (Madec 2015).

EC-Earth3-CC describes the carbon cycle and is used for the Coupled Climate-Carbon Cycle Model Intercomparison Project (C4MIP; Jones et al., 2016). The configuration allows for concentration driven simulations and with emissions forcings. The $CO_2$ flux is calculated from and proportional to the difference in partial pressure of ($\Delta pCO_2$) between the atmosphere and the surface of the ocean (Döscher et al., 2022).

EC-Earth3-CC runs with NEMO3.6 coupled to PISCES-v2 (Pelagic Interactions Scheme for Carbon and Ecosystem Studies volume 2; Aumont et al., 2015), a biogeochemical model simulating marine biological productivity and the biogeochemical cycling of carbon and the main nutrients. Primary productivity is computed based on the availability of the main nutrients (P, N, Si, Fe), with a constant Redfield ratio (P : N : C = 1 : 16 : 122) (redfield ratio from Takashi et al., 1985; Aumont et al., 2015). Air-sea gas exchange for carbon dioxide is parameterised from Wanninkhof (1992), updated in Wanninkhof (2014) to Eq 1:

$$F = k\,K_0(pCO_{2w} - pCO_{2a}) \tag{1}$$

where F is the flux (mass area$^{-1}$ time$^{-1}$), k is the gas transfer velocity (lenght time$^{-1}$) and $K_0$ is the solubility (mass volume$^{-1}$ pressure$^{-1}$), which is dependent on water temperature and salinity, $pCO_{2w}$ and $pCO_{2a}$ (pressure) are the partial pressures of $CO_2$ in equilibrium with surface water and the above lying air, respectively. The gas transfer velocity is dependent on wind speed according to Eq. 2:

$$k = 0.251\,U^2 \left(\frac{Sc}{660}\right)^{-0.5} \tag{2}$$

where U is the wind speed (10 m height), Sc is the Schmidt number. The Schmidt number is dependent on water temperature. Furthermore, the $CO_2$ flux is dependent on the SIC in the region, as no exchange is allowed between the atmosphere and sea water across sea ice Eq. 3:

$$kgCO_2 = k'gCO_2 \times (1 - \%_{ice}) \tag{3}$$

where kgCO2 is the atmosphere–ocean $CO_2$ flux after correcting for the SIC, k'gCO2 is the atmosphere–ocean $CO_2$ flux before correcting for SIC, %$_{ice}$ is the concentration of sea ice which varies between 0 and 1 (Döscher et al., 2022, Aumont et al, 2015).

The present day (1982-2014) averaged air-sea $CO_2$ flux shows a general flux into the ocean in the North Atlantic and Nordic Seas (positive $CO_2$ flux, Fig 1a-c). Observations show a similar pattern of a positive flux ($CO_2$ uptake in the ocean) in the North Atlantic and Arctic region, and a negative flux (outgassing to the atmosphere) off the western coast of Africa across the Atlantic and off the coast of South America (Fig 1b). However, observations generally show a smaller air-sea $CO_2$ flux than simulated in EC-Earth3-CC (Fig 1c). Döscher et al. (2015) shows that the EC-Earth3-CC air-sea $CO_2$ flux is in general overestimated in the high northern latitudes (>50°N) in the northern hemisphere, and underestimated in the high latitudes in the southern hemisphere. However, the general distribution of the air-sea $CO_2$ flux is well represented in EC-Earth3-CC (Fig 1a-c).

The sea ice extent of EC-Earth3 (and therefore also EC-Earth3-CC) is in general overestimated in the Nordic Seas (NS) and NA compared to observations (Döscher et al., 2022; Tian et al., 2021). As no exchange between the atmosphere and seawater is allowed across sea ice in EC-Earth3, an overestimation of the sea ice extent will inevitably affect the $CO_2$ flux. The global pattern of the $CO_2$ flux and the overestimation of the sea ice extent emphasises the importance of sea ice and high latitude processes in the global climate system (Fig. 1).
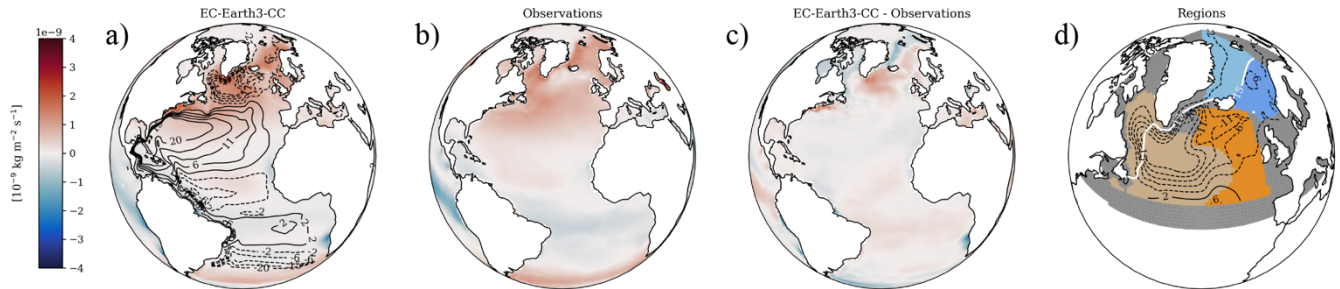
**Figure 1: Atmosphere–ocean $CO_2$ flux averaged over the period 1982-2014 for a) EC-Earth3-CC, b) observation based reconstruction $CO_2$ flux data from Gregor and Fay (2021), c) their difference. Black lines show the mean barotropic streamfunction of the SPG circulation of ten ensemble members in Sv. Full line indicating positive values, dashed line indicating negative values. Closed dashed lines show the mean extent of the SPG. d) study regions: NA covering all regions (dark grey) SPW (beige), SPE (orange), NSE (blue), NS covering NSE as well (light blue), global average 15% SIC line (white contour) indicating the boundary between sea ice covered regions and sea ice free areas.**

## 2. Data and methods

The analysis is based on EC-Earth3-CC historical runs 1850-2014 from all available ensemble members on ESGF (*https://aims2.llnl.gov/search/cmip6/*) (ten ensemble members: r1i1p1f1, r4i1p1f1, r6i1p1f1, r7i1p1f1, r8i1p1f1, r9i1p1f1, r10i1p1f1, r11i1p1f1, r12i1p1f1, r13i1p1f1). We make use of monthly mean fields of the parameters shown in Table 1. The data is preprocessed pointwise for analysis on two seperate timescales: decadal and interannual. For the decadal timescale a

10 year low-pass filter (using CDO, filtering the data in the frequency domain: Schulzweida et al., 2012) has been applied to the data. Following the low-pass filtering the data has been linearly detrended to remove the anthropogenic forced changes due to increases in atmospheric greenhouse gases and to be able to focus on the internal climate and ocean variability of the North Atlantic. The atmosphere–ocean $CO_2$ flux (and $\Delta pCO_2$) shows a modest linear increase from 1850–1950 and then a transition to a steeper increase until 2015 (see also section 2.2, Fig. 2). Therefore, in this case a two step piecewise linear fit has been used to detrend the dataset. The model dataset has been detrended along the time axis for every grid cell, allowing for analysing the detrended data on a regional scale. Other parameters have been detrended using a linear fit. We choose not to apply any detrending to the streamfunction data at grid point level. A second preprocessed dataset of interannual variability is prepared by subtracting the low-pass filtered timeseries from the original model data. Also here, the interannual $CO_2$ flux and $\Delta pCO_2$ dataset has likewise been detrended using a two-step linear fit, and other parameters using a linear fit.

**Table 1**

Parameters from EC-Earth3-CC

| Parameter | Output variable name | Form of detrending | Unit |
|---|---|---|---|
| $CO_2$ flux | fgco2 | two-step linear | $kg\ m^{-2}\ s^{-1}$ |
| $\Delta pCO_2$ | dpco2 | two-step linear | Pa |
| Sea surface temperature (SST) | tos | linear | °C |
| Sea surface salinity (SSS) | sos | linear | |
| Wind | sfcWind | linear | $m\ s^{-1}$ |
| Mixed layer depth (MLD) | mlotstmax | linear | m |
| Sea surface height (SSH) | zos | linear | m |
| Sea ice concentration (SIC) | siconc | linear | % |
| Pressure at sea level | psl | linear | Pa |
| AMOC | msftyz | None | $kg\ s^{-1}$ |
| Barotropic mass streamfunction | msftbarot | None | $kg\ s^{-1}$ |

## 2.1 Regions

This study looks into the $CO_2$ flux variability in multiple regions in the North Atlantic (Fig. 1b), to investigate the regional differences in the relationship between the $CO_2$ flux and the physical and dynamical processes. The geographic regions are defined considering the model representation of oceanographic domains. The North Atlantic (NA) region covers all of the ocean in the region 40°N - 90° N, -78°W - 45° W, with avereage ocean $CO_2$ uptake. The Nordic Seas (NS) is defined roughly where warmer subpolar North Atlantic waters in the model meets waters of the Nordic Seas at the latitude of the

Greenland Scotland Ridge and defined as the region 60°N - 90° N, 28°W - 18°W. The Nordic Seas east (NSE) is defined as the NS, but only where model climatology has less than 15% sea ice and as such, representing the sea ice free part of the NS, allowing for unbiased investigation of the dynamics not related to the overestimated sea ice extent. The Subpolar region of the North Atlantic is divided into two oceanic domains: the Subpolar West (SPW) and the Subpolar East (SPE). The SPW is defined as where the annual mean SSS is <34.2 within the region 45°N - 60°N, 52°W -10°W, the part of the subpolar gyre recirculating watermasses modified by low salinity polar outflow and melting sea ice. The SPE is defined as SSS >34.2 within the region 45°N - 64°N, 52°W - 10°W in the path of the North Atlantic current. The SPE, like the NSE, represents a region with no sea ice cover (climatological SIC <15%).

## 2.2 $CO_2$ flux variability

**Table 2**
Variability (standard deviation, std) of ensemble mean $CO_2$ fluxes for F (model output), $F_{calc}$ (calculated flux) in interannual (int) and decadal (dec) timescales

| Std | F [$10^{-11}$ kg m$^{-2}$ s$^{-1}$] | | $F_{calc}$ [$10^{-11}$ kg m$^{-2}$ s$^{-1}$] | | Area of region [$10^{12}$ m$^2$] |
|---|---|---|---|---|---|
| | Int | Dec | Int | Dec | |
| NA | 3.22 | 2.16 | 2.92 | 2.39 | 11.27 |
| NS | 5.35 | 5.87 | 5.05 | 5.56 | 0.96 |
| NSE | 8.23 | 6.99 | 7.08 | 5.93 | 0.27 |
| SPW | 8.22 | 5.49 | 7.52 | 5.28 | 2.86 |
| SPE | 6.85 | 5.84 | 5.96 | 4.97 | 1.04 |

Archived climate model data available from CMIP6 on the ESGF nodes typically consists of monthly mean fields of physical, biological and chemical parameters. This includes surface air sea $CO_2$ fluxes from EC-Earth3-carbon cycle as well as ocean properties. The reproducibility of simulated integrated fluxes (F) derived from other parameters (Eq. 1-3), particularly their variability across different timescales, provides a useful benchmark. It sets an upper limit on how much of the model variability we can expect to explain using physical quantities from archived monthly-averages data. Figure 2 also shows the time evolution of $F_{calc}$ ($CO_2$ flux calculated according to Eq 1-3) of a selected ensemble member (r4i1p1f1) and for the NS, NSE and SPE region only. To accurately reproduce the simulated flux, $F_{calc}$ is computed using a scaled wind speed. Since $F_{calc}$ is derived from monthly mean values of all parameters, some of the short-term variability in dynamic factors—particularly wind speed— is smoothed out, leading to a lower mean wind speed compared to the daily mean used in EC-Earth3-CC. Hughes et al. (2012) discusses a averaging-related bias linked to ocean surface flux calculations and show that the use of monthly mean fields can introduce a bias into the mean flux estimates (also discussed by Esbensen and Reynolds, 1981; Simmonds and Dix 1989; Gulev, 1994; 1997; Josey et al., 1995; Zhang 1995; Esbensen and McPhaden 1996; Simmonds and Keay 2002). Given that

Eq. 2 shows a nonlinear dependence of $CO_2$ flux on wind speed ($U^2$), even small-scale wind variability can have a significant impact on flux calculations. To account for the reduced wind variability in the monthly mean fields and ensure consistency with the original flux calculation, a scaling factor of 1.2 is applied to the wind speed when computing $F_{calc}$. The scaled wind is only used for this calculation and not in any of the other analyses. It is also expected that the $CO_2$ flux variability is dependent on SST and SSS variability, however the effect of SST and SSS on the solubility constant ($K_0$) is too small to be considered important in these calculations, and the SST and SSS components of Eq 1-3 is therefore not scaled. The absolute level of the $F_{calc}$ compared to the model flux is well captured including the trend. For this ensemble, the correlation between the estimated flux and the model output in SPE exceeds 0.9 ($R^2$) with a regression factor close to unity (1.1). We find comparable/significant skill in reproducing fluxes for the shorter timescale (not shown).

Figure 2 shows the average (weighted mean) $CO_2$ flux time series F for each region with interannual variability removed. The anthropogenic trend is evident in all regions including the accelerated trend after 1950. Differences between regions are evident with NSE showing the largest $CO_2$ uptake per unit area. Strong decade-scale variations do modulate regionally the accelerated trend after 1950 emphasizing the importance of ocean variability. Removing the anthropogenic trend and isolating interannual and decadal variability reveals i) relatively comparable levels of variability across regions and ii) a stronger variability on short timescales (Table 2). Ensemble mean results indicate that NSE, which is also the smallest area, is subject to strongest variability on both timescales, followed by the SPW (Table 2).
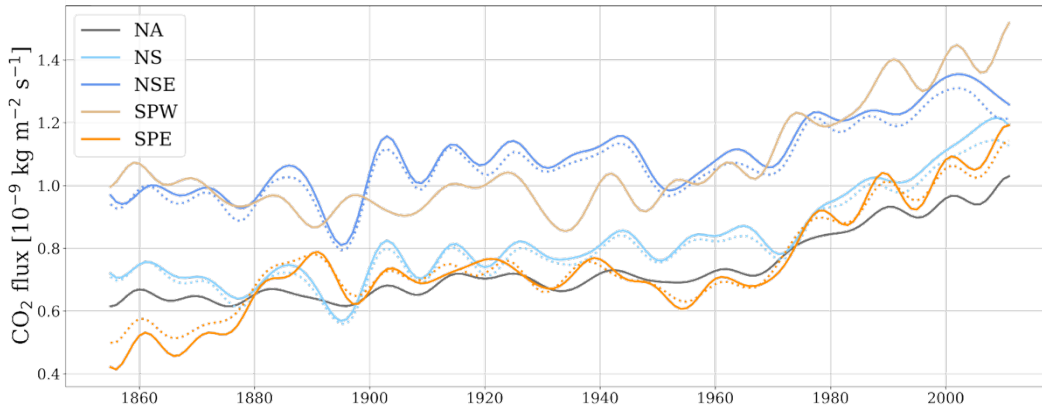
**Figure 2: Decadal variability in the simulated $CO_2$ flux (F, solied line) and calculated flux ($F_{calc}$, dotted line) for ensemble member r4i1p1f1. Here the weighted mean is shown to compare the fluxes and variability across regions. $F_{calc}$ only showed for NS, NSE, SPE**

## 3. Results

### 3.1 Regional $CO_2$ flux variability

To visualise the patterns of $CO_2$ flux variability across timescales and regions, we create composite maps of the $CO_2$ flux and the parameters we expect to be important drivers of the variability. These parameters include parameters already presented above (SST, SSS, SIC, $\Delta pCO_2$ and wind), however for the next part of the analysis we add mixed layer depth (MLD) and sea

surface height (SSH). These parameters represent larger scale dynamics such as ocean circulation (SSH, gyre strength) and vertical mixing (MLD), which are candidates to be indirect processes controlling the $CO_2$ flux variability in EC-Earth3-CC. After detrending the data as described above, we define high and low $CO_2$ flux years in the different study regions based on

250    the mean standard deviation for all the ten members (+/-) one std from the regional mean. The years are defined and selected for each member for all the parameters, where after the difference of the ensemble mean high minus low flux years is shown in composite maps (Fig. 3-7).

       The North Atlantic region covers all the other regions. The $CO_2$ composite maps show a widespread homogeneous pattern of $CO_2$ uptake, intensified across the subpolar region (Fig. 3) and with regional differences. This includes the

255    Irminger and Iceland Basins, where fluxes are moderated and locally reversed. On decadal timescales, positive values (increased $CO_2$ uptake) are confined to areas near the sea ice edge indicating that this exerts significant control over North Atlantic average $CO_2$ flux variability at longer timescales (Fig. 3b). On interannual timescale, the widespread $CO_2$ uptake mirrors a widespread pattern of stronger winds and colder SST, indicating that these parameters are potential drivers of the $CO_2$ flux variability on shorter timescales. This is not the case for decadal variability where only positive wind speed project

260    on regions of enhanced $CO_2$ flux, temperature generally warm and act to reduce solubility. A positive $\Delta pCO_2$ pattern compares spatially with the positive $CO_2$ flux anomaly and negative SST anomaly (Fig. 3a). On the decadal timescale, a negative SSH anomaly, indicating a strengthening of the subpolar gyre, compares spatially with the positive $CO_2$ flux anomaly in the subpolar gyre region, which suggest that the strength of the subpolar gyre also could be a potential dynamical driver of the $CO_2$ flux variability, modifying key parameters like SST and SIC. The $CO_2$ flux variability pattern in the North

265    Atlantic appears relatively homogenous, while its comparisons with other parameters are less distinct, except for SST on short timescales and SIC on long timescales. This suggests that multiple dynamics may be influencing $CO_2$ flux variability. To better understand these influences, we will analyse smaller, well-defined regions to identify the key drivers of $CO_2$ flux variability.

270
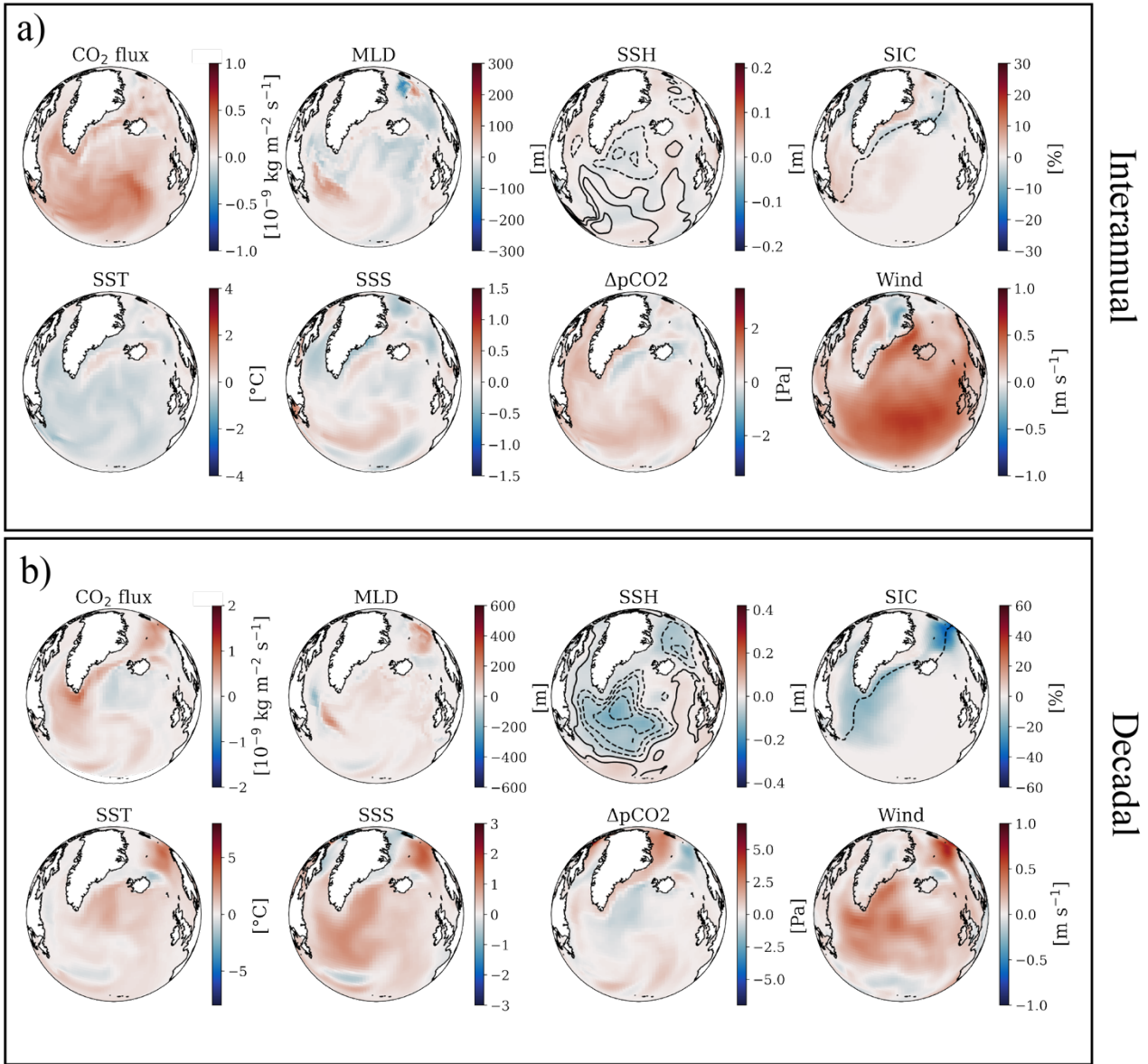
**Figure 3 Anomalies of the high-low years of the dynamic parameters compared to the CO₂ flux anomaly in the NA. a) showing interannual timescale and b) showing decadal timescale. Full and dashed lines on top of the SSH anomaly shows the barotropic mass streamfunction anomaly and dashed line on top of SIC anomaly shows the 15% SIC climatology (mean of ten ensemble members on both timescales).**

Focusing in on the the Nordic Seas region, we see a widespread and homogeneous pattern of $CO_2$ uptake on interannual timescale (Fig. 4), on short timescales confined to the Nordic Seas emphasising the role of regional dynamical systems and need for a regional analysis. The Nordic Seas shows the strongest flux anomalies across all the regions, in particular on long timescales. On decadal timescales, the $CO_2$ uptake is confined to an area of varying SIC in the Nordic Seas with dynamical

consistent patterns also in the SPG region, indicating that SIC is the main driver of the $CO_2$ flux variability in this region on
longer timescale (Fig. 4a). Positive SST anomalies reaching 5°C on decadal scale would counteract the effects of sea ice
variability. On the shorter timescale, the $CO_2$ uptake is enhanced  across most of the Nordic Seas region, however, on
decadal scale a small part of the region shows $CO_2$ outgassing (Fig. 4b), likely linked to the strong warming of the composite
and reduced $\Delta pCO_2$. Again, the positive $CO_2$ flux anomaly is perfectly confined to areas within an area of decrease in SIC,
indicating that SIC is the main driver of $CO_2$ flux variability on the shorter timescale as well. The decrease in SIC is greater
in the Nordic Seas composite maps compared to the North Atlantic maps. On both timescales stronger winds compare
spatially with the increased $CO_2$ uptake, similar to the North Atlantic region. However, the wind anomaly is stronger on the
longer timescales compared to the shorter timescales. Following a decrease in SIC we see a deepening of the MLD due to
increased convection, increasing the mixing and allowing for an increase in air-sea $CO_2$ flux. However, the small scale and
spatial pattern associated with enhanced mixing is not obviously reflected in the patterns of $CO_2$ uptake. Also, from the
spatial comparison of patterns, it is clear that $\Delta pCO_2$ changes alone cannot explain the $CO_2$ flux variability.

285

290

295
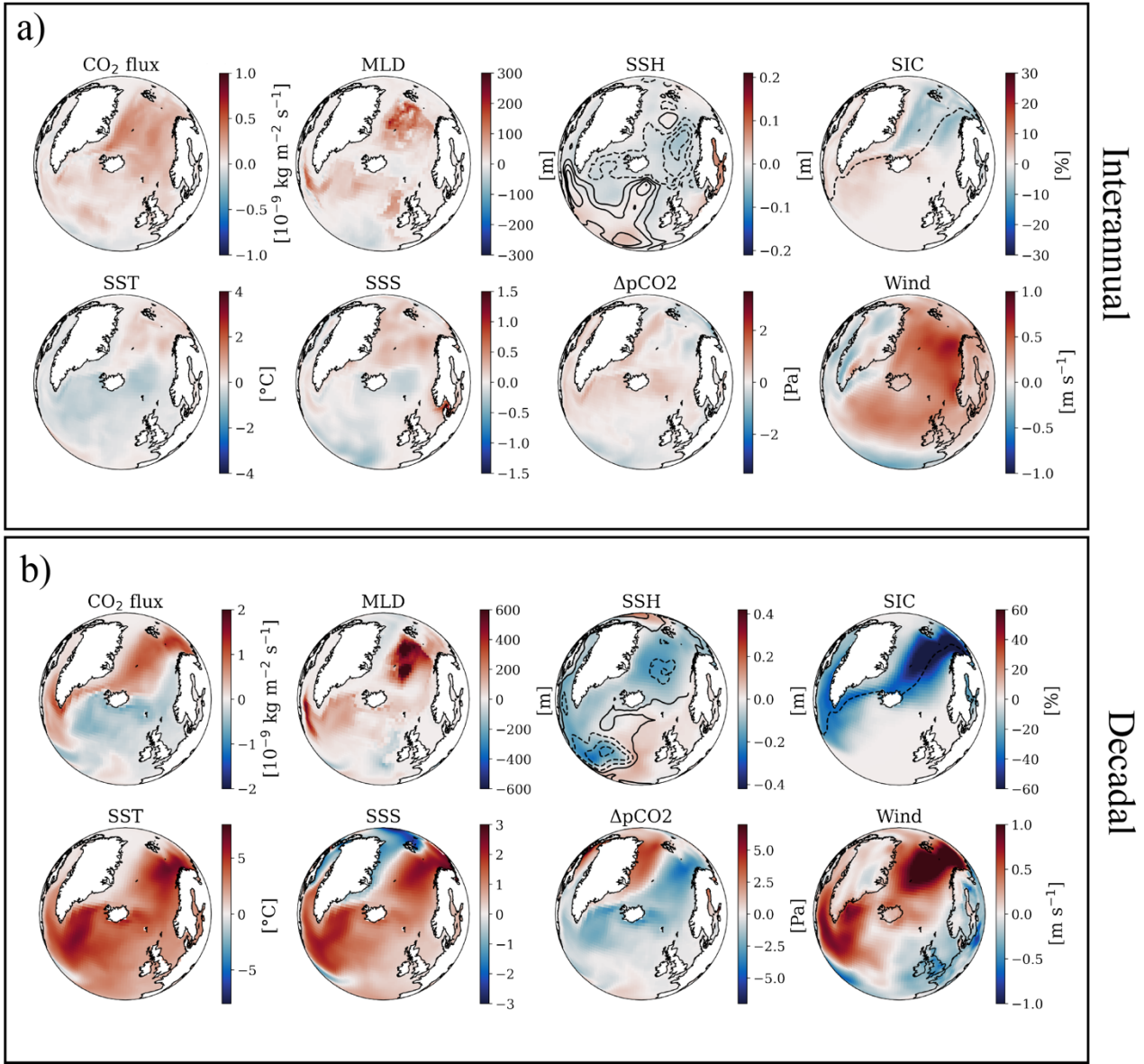
**Figure 4 Anomalies of the high-low years of the dynamic parameters compared to the CO₂ flux anomaly in the NS. a) showing interannual timescale and b) showing decadal timescale. Full and dashed lines on top of the SSH anomaly shows the barotropic mass streamfunction anomaly and dashed line on top of SIC anomaly shows the 15% SIC climatology (mean of ten ensemble members on both timescales).**

The Nordic Seas East region represents the sea ice free part of the Nordic Seas (less than 15% SIC) and is in the path of the North Atlantic current crossing the Greenland Scotland Ridge. The composite maps of high minus low CO₂ flux years show an increased CO₂ uptake (Fig. 5) confined to the NSE region highlighting that our regionalisation is relevant and allow us to

isolate a dynamical regime. The region is confined by the 15% SIC line, and shows a widespread positive $CO_2$ flux anomaly. Figure 5a illustrates that the interannual variability shows an increase in wind which compares spatially with a deepening of the MLD and an increase in the air-sea $CO_2$ flux. These patterns are more pronounced for the NSE than for the NS region. A decrease in SSH indicates a strengthening of the Nordic Seas gyre circulation, the eastern part, mirroring an increase in MLD and $CO_2$ flux indicating a dynamic driver of the $CO_2$ flux variability. Figure 5b shows a confined pattern of $CO_2$ uptake, which compares spatially with a confined pattern of stronger wind, increased MLD as a result of a strengthening of the Nordic Seas Gyre (NSG; shallowing of the SSH) and increased SSS. Compared to the North Atlantic region, the Nordic Seas East gives a clearer indication of the driving forces behind the $CO_2$ flux variability.
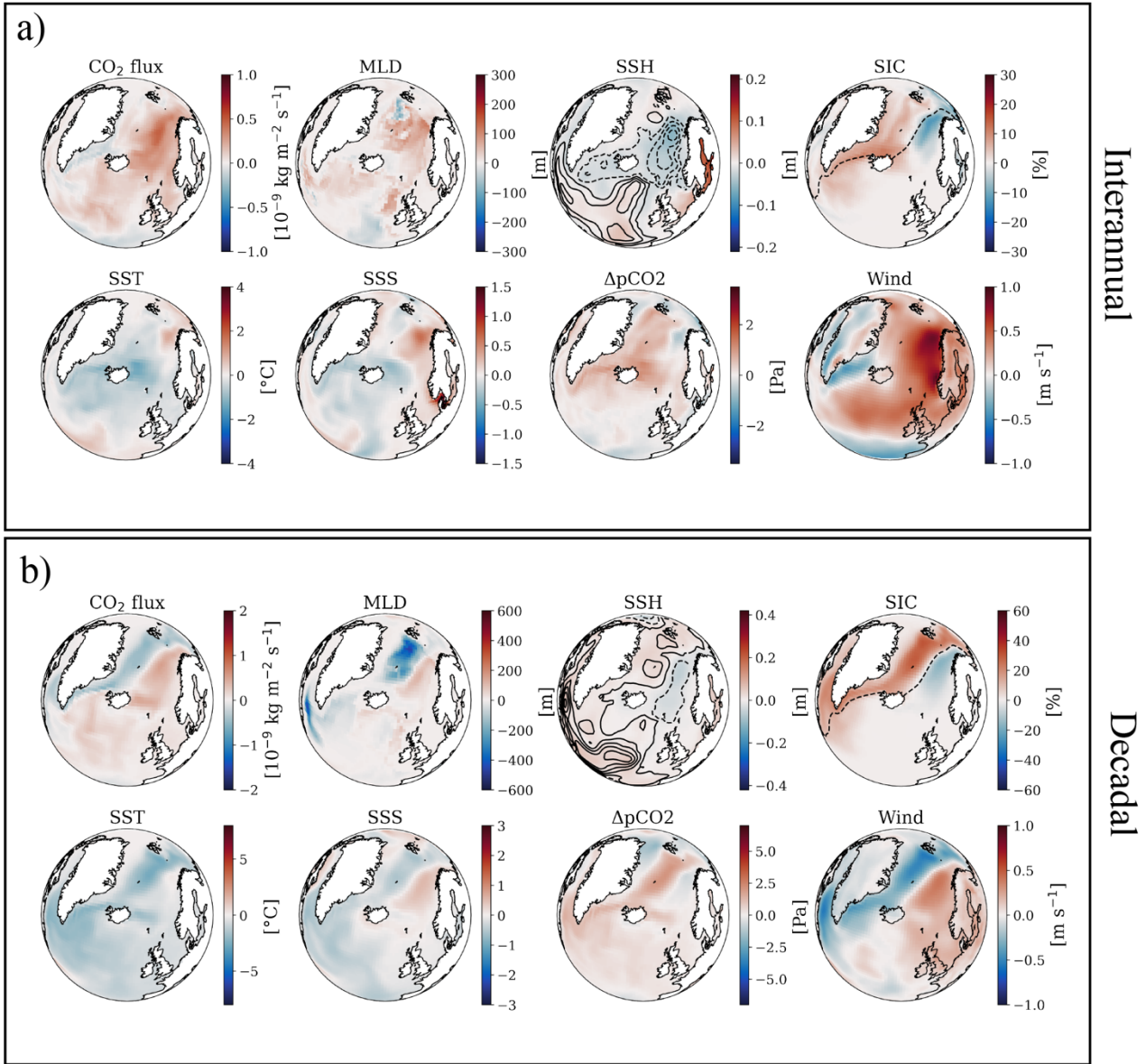
**Figure 5 Anomalies of the high-low years of the dynamic parameters compared to the CO₂ flux anomaly in the NSE. a) showing interannual timescale and b) showing decadal timescale. Full and dashed lines on top of the SSH anomaly shows the barotropic mass streamfunction anomaly and dashed line on top of SIC anomaly shows the 15% SIC climatology (mean of ten ensemble members on both timescales).**

In the western part of the subpolar region, the CO₂ flux spatial pattern is strikingly similar to the pattern we can construct for the entire North Atlantic on both timescales (Fig. 3 and 6). This can in part be expected from the vast area of the region hereby dominating the area-averaged fluxes and composites. Key differences with the NA region includes the Irminger Sea where also SSH patterns indicate a dynamical separation on interannual scales. On the interannual timescale the region

shows $CO_2$ uptake within the full region (Fig. 6a), whereas the decadal $CO_2$ flux shows both positive and negative anomalies within the region (Fig. 6b). In general all the parameters show similar patterns to the North Atlantic on both timescales.

325 However, on the interannual timescale we see a more clear and confined signal from SST and SSS compared to the North Atlantic. A negative SST anomaly compares spatially with increased $CO_2$ uptake in the full region, whereas a positive SSS anomaly in most of the region shows a relationship with the $CO_2$ flux variability, emphasising how the SSS can work as an indirect driver or indicator. On the decadal timescale we see a clear and confined signal in the indicated drivers of the $CO_2$ flux compared to the North Atlantic region. Here, we see that the $CO_2$ uptake is confined within the region of decreasing

330 SIC, indicating that SIC forces a main control on the $CO_2$ flux variability in the region. Furthermore, we see a greater strengthening of the subpolar gyre as indicated by the decrease in SSH on both timescales, however the strongest signal is seen on the longer timescale, where we also see a shift towards the east as expected in a strong SPG phase. The strengthening of the subpolar gyre results in a deepening of the MLD and introduces more saline Atlantic Water into the system from further south, which explains why we see a positive SSS anomaly and increased $CO_2$ uptake. As in the North

335 Atlantic region, we see opposite anomalies for the SST on the two timescales. A negative SST anomaly mirrors a positive $CO_2$ flux anomaly on the short timescale, whereas on the longer timescale, we see a positive SST anomaly and a positive $CO_2$ flux anomaly.

# Subpolar West
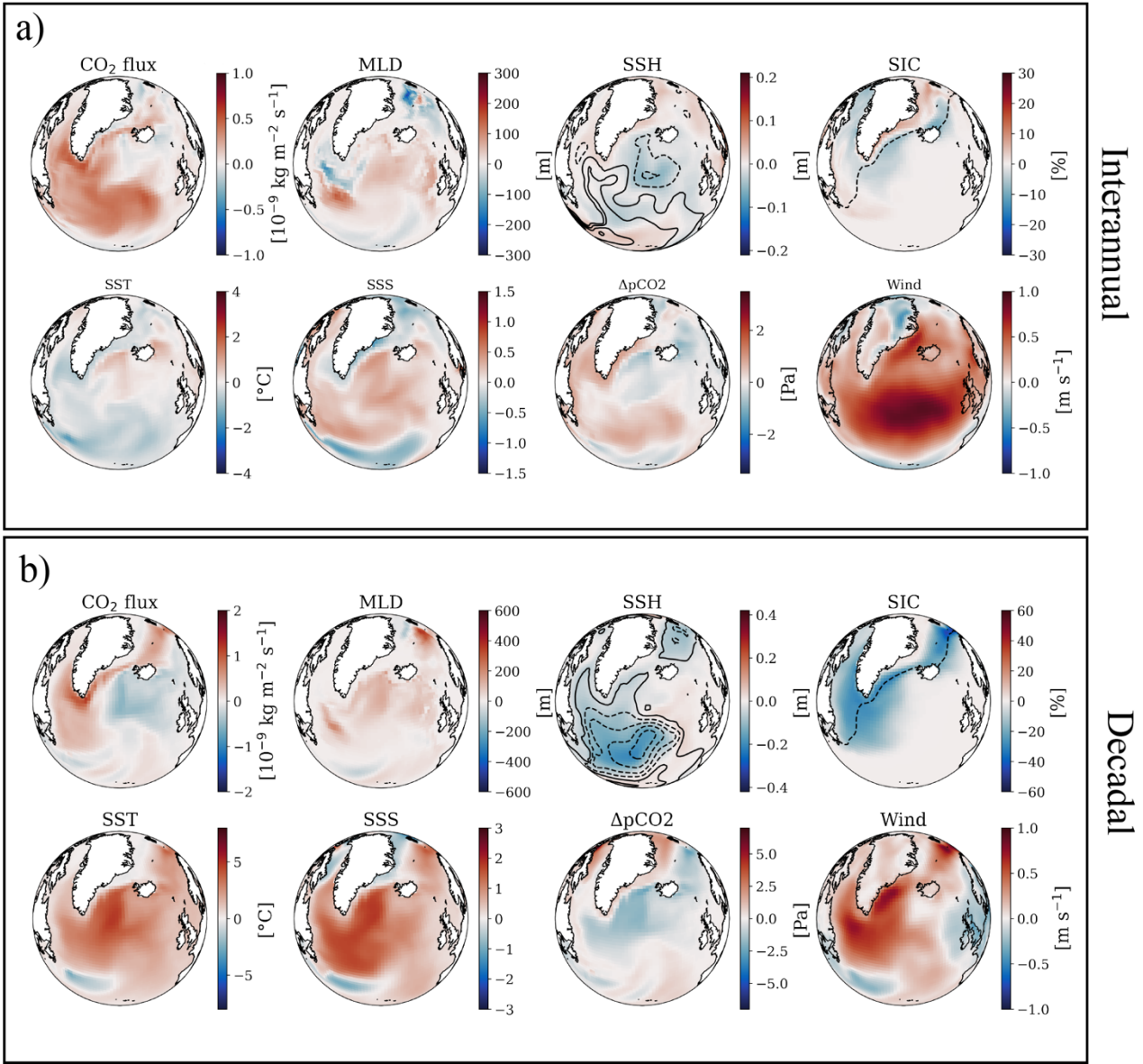
**Figure 6 Anomalies of the high-low years of the dynamic parameters compared to the CO₂ flux anomaly in the SPW. a) showing interannual timescale and b) showing decadal timescale. Full and dashed lines on top of the SSH anomaly shows the barotropic mass streamfunction anomaly and dashed line on top of SIC anomaly shows the 15% SIC climatology (mean of ten ensemble members on both timescales).**

Lastly, we look at the eastern part of the subpolar region (Fig. 7). The composite maps show patterns of increased $CO_2$ uptake, which is regionally well confined to the eastern subpolar gyre and not apparently analogue to the composite patterns derived for SPW. This includes also the North Atlantic region. On the interannual timescale SSH reflects what may best be

350 characterized as a relative blocking of the path of the North Atlantic current (a closed gyre system building up sea surface height). On the decadal timescale this blocking cell is located further south, outside of the SPE region, but in both cases result in cooling of the wider subpolar region as well as freshening. Despite these basin wide linkages, the $CO_2$ flux changes are regionally exaggerated in the SPE. Not surprisingly, the dynamical changes – a blocking of the path of the North Atlantic current – are also characteristic of the composite maps for the NSE region (Fig. 5). Despite this apparent similarity, the $CO_2$

355 flux patterns are in both cases not extending across the Greenland Scotland Ridge. This may be explained by phase differences in the impacts.

The spatial pattern of positive $CO_2$ flux anomaly reflects a shallowing of the MLD on the interannual timescale. This cannot directly be linked to increased uptake, on the contrary as described in section 1 and 3.1, as a shallowing of the MLD is related to a less ventilated water column, and thereby a decrease in the $CO_2$ uptake. This link is discussed further in

360 the next section. Also on the interannual timescale, a positive wind anomaly, and a negative SST and SSS anomaly also align spatially with positive $CO_2$ flux anomalies. On the decadal timescale, the signal from the MLD and wind is less clear, however, a negative SST and SSS anomaly compares spatially with the increased $CO_2$ uptake in the region.

## Subpolar East
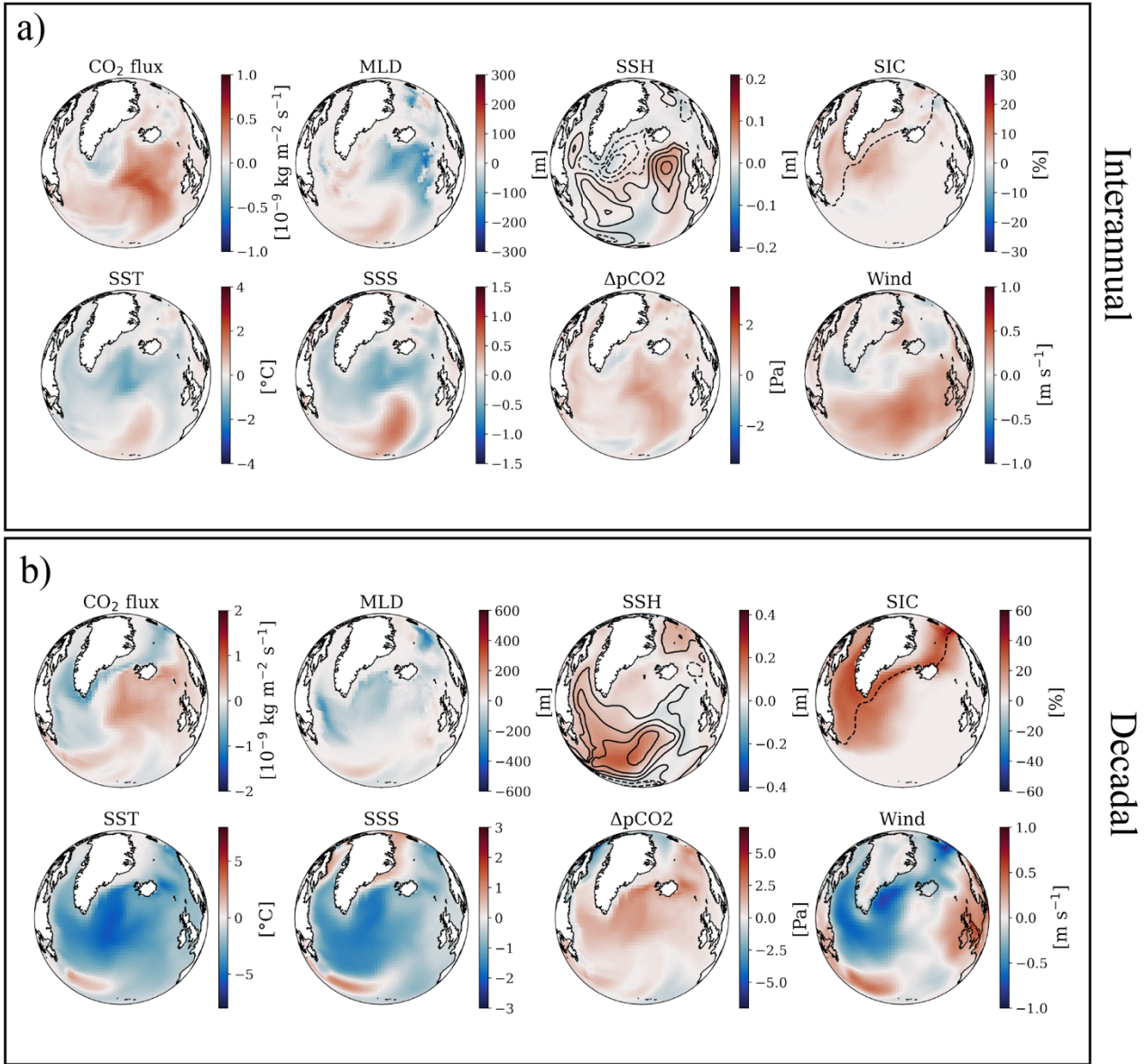
365 **Figure 7 Anomalies of the high-low years of the dynamic parameters compared to the CO₂ flux anomaly in the SPE. a) showing interannual timescale and b) showing decadal timescale. Full and dashed lines on top of the SSH anomaly shows the barotropic mass streamfunction anomaly and dashed line on top of SIC anomaly shows the 15% SIC climatology (mean of ten ensemble members on both timescales).**

## 3.2 Ocean indexes

Following the qualitative discussion of the relationship between the $CO_2$ flux variability and the dynamical parameters on different timescales, we define integrated quantities and make use of ocean indicators such as the subpolar gyre index to understand statistical significance of the identified relationships between the $CO_2$ flux and ocean variability (Table 3).

The Subpolar Gyre index (SPGi) is here defined simply as the minimum SSH of the NA region. This differs from other definitions (Hátún et al. 2005, Berx and Payne et al., 2017) but captures the main variability of the Earth System Model analysed. The index is inverted, meaning that a positive (negative) anomaly indicates a strong anticyclonic (weak) SPG. The subpolar gyre index describes not only the state of the subpolar region but from observations also shown to characterize variability in water mass properties at the gateways to the Nordic Seas (Hátún et al., 2005; Hátún et al 2017). As such, the SPGi may be linked to $CO_2$ flux variability directly by describing the extent of the characteristic colder and fresher subpolar upper ocean water masses and indirectly through correlations with other drivers such as variability in sea-ice margins, wind stress and ocean mixing locally and remote (Nordic Seas). From correlation coefficients (zero lag) between the SPGi with the $CO_2$ flux anomaly for the different regions (NA, NS, NSE, SPW, SPE), presented in Table 3, it is clear that the SPGi does not explain the $CO_2$ flux variability on the interannual timescale very well, though reassuringly the highest correlation are found for the SPW region. The SPGi correlates better on the decadal timescale, with an ensemble mean of 0.31 and 0.44 in the NA and SPW respectively. Several ensemble members show a correlation coefficient of 0.4 or higher in both regions, but a few ensemble members show very low correlation, resulting in reduced ensemble mean values. The SPE shows a large spread in individual ensemble correlations with both positive and negative correlations, resulting in an ensemble mean of -0.24 and -0.17 (interannual and decadal, respectively). The low degree of correlation on both timescales is expected in part due to the finding from the composite map analysis of a more regional SSH (and streamfunction) 'blocking pattern' of the North Atlantic Current.

The Nordic Seas Gyre index (NSGi) is defined as the minimum SSH in the NS region, similar to the SPGi. The index is inverted, meaning that a positive value indicates a strong anticyclonic gyre circulation, whilst a negative value indicates a weakening of the gyre circulation. The NSGi will be modulated by changes in wind stress curl and also not independent of other possible indices defined on the basis of MLD and SIC. We have no a-priori expectation of a strong relation between the NSGi and $CO_2$ flux in other regions. The NSGi correlates well with the $CO_2$ flux variability in the NS on the decadal timescale (0.54, Table 3), but also on the interannual timescale (0.30, Table 3). A strong (weakened) NSGi results in an increased (decrease in) $CO_2$ uptake in the ocean. Hátun et al. (2021) shows that a strong NSG circulation results in an uplifted thermocline, which results in more ventilation of deeper water. The ventilation of deeper water could lead to an increased air-sea $CO_2$ flux, and work as a driver for the increased $CO_2$ uptake in the NS. The composite maps show a strengthening of the NSG (deepening of the SSH) on both timescales, however a greater strengthening on decadal timescale, indicating that a strengthening of the NSG could result in an increased atmosphere–ocean $CO_2$ flux.

The AMO index is defined as the anomaly of the mean SST in the NA region. For the regions within the NA, the index is defined as a SST index, which is the anomaly of the mean SST within the region. We have chosen to use the SSTi for the smaller regions, to investigate the direct relationship of SST and $CO_2$ flux variability within the regions. A positive AMO/SSTi phase describes a warming of the North Atlantic. As higher SST's increase the $pCO_2$ in the ocean due to lower solubility, the AMO should be negatively correlated to the $CO_2$ flux. However, Breeden and McKinley (2016) shows how a positive AMO phase results in a decrease in DIC in the SPG, which decreases the solubility and increases the $fCO_2$ (and the $pCO_2$). On the decadal timescale we see that the $CO_2$ flux variability in NS and SPW region correlates positively (0.36 and 0.29, Table 3) with the SSTi, which can be related to the dynamics explained by Breeden and McKinley (2016). Also, an increase in temperature in the NS would result in a decrease in SIC, allowing for an increase in $CO_2$ flux. Breeden and McKinley (2016) states that SST and the solubility of $CO_2$ in the ocean still affects the $pCO_2$ in the ocean (and thereby the air-sea $CO_2$ flux), but that the biogeochemical dynamics, such as DIC are of a stronger amplitude. The NSE and SPE regions shows an inverted correlation between the $CO_2$ flux variability and the SSTi on both timescales (NSE: -0.12 and -0.41 SPE: -0.15 and -0.38, interannual and decadal), indicating that the temperature effect on the $CO_2$ solubility in the surface ocean dominates the $CO_2$ flux variability in these regions (Table 3). In the NA the degree of correlation varies a lot between the ensemble members from a negative/weak correlation to a stronger correlation, which makes it difficult to say anything in general about the full NA region.

The sea ice index (SIi) is defined as the SIC anomaly in the specified regions. An increase in SIC results in a decrease in $CO_2$ flux into the ocean in case no other factors are changing. In the NS the SICi in general has a strong negative correlation with the decadal $CO_2$ flux anomaly, all of the members showing a correlation coefficient above 0.50, resulting in an ensemble mean of -0.64 (Table 3). The interannual variability in the NS shows a lower correlation, with an ensemble mean of -0.36 (Table 3). On both timescales, the SPW region shows a weaker negative correlation compared to the NS (-0.04 and -0.36, interannual and decadal), as expected due to a smaller degree of sea ice extent in the SPW. However, it is clear that the SIC is still dominating the $CO_2$ flux variability in this region. The NA region shows the weakest correlation between the SICi and the $CO_2$ flux variability, which migth be explained by the fact that the sea ice covered region of the NA is small (-0.02 and -0.26 interannual and decadal). The SICi has not been applied to the NSE and SPE regions, as they are more or less sea ice-free.

The NAO index is defined as the atmospheric surface pressure level anomaly between Iceland (65° N, 20° E) and the Azores (40° N, 25° E) in the winter months (djfm; Hurrel 1995). The correlation between the NAO and $CO_2$ flux is in general strongest on the interannual timescale, showing a correlation coefficient of around 0.3 for most regions, except SPE that shows 0.12 and 0.35 interannual and decadal, respectively. On the decadal timescale the ensemble mean correlations are weaker, however in particular in the ice-free SPE and NSE and in the NA some ensemble members show a correlation of 0.4-0.5 (Table 3). The NAO and associated wind stress and wind stress curl impacts the ocean dynamics of the region including sea ice distribution which may explain the positive correlations, whereas the direct effects of changes in wind stress on gas transfer would be expected to result in negative correlations for some regions.

The AMOC index (AMOCi) is defined as the anomaly of the maximum of the model Atlantic Meridional Overturning Circulation (streamfunction) at 45°N in the top 1000m of the water column. We choose 45°N to align with the boundary of the Subpolar and subtropical gyres and reduce potential time lag, that would follow from using an index defined at lower latitudes. On the interannual timescale, the AMOCi shows a strong negative correlation in the NA and SPW regions (-0.40 and -0.47, Table 3), indicating that a weakened AMOC resulting in less heat transport to the Northern North Atlantic will result in increased ocean $CO_2$ uptake. In the other regions, the ensemble members show a low correlation on the short timescale. On the decadal timescale, somewhat surprisingly, the AMOCi is not as closely and directly related to surface $CO_2$ exchange with both negative and positive correlation coefficients in all the regions, resulting in a weak average correlation (Table 3).

The wind index (Wi) is defined as the anomaly of the average near surface (10 m) wind speed in the different regions. As expected based on Eq. 2, the Wi correlates positively with the $CO_2$ flux variability for all regions independent on timecale. On both interannual and decadal timescale, the Wi shows a high correlation with the $CO_2$ flux in the NA (0.68 and 0.45), NS (0.73 and 0.70) and NSE (0.72 and 0.57, Table 3). However, SPW only shows a high correlation on an interannual timescale (0.80 and 0.26 decadal), whereas SPE shows a weaker correlation on both timescales (0.24, 0.26). In the composite maps all the regions show a strong positive wind anomaly, whereas the SPE region shows a weak positive anomaly on the interannual timescale and a mix of negative and positive anomalies on the decadal timescales, which might explain the weak correlation seen in the region.

To understand the dynamic process of upper ocean mixing and its effect on the atmosphere–ocean $CO_2$ flux variability a MLD index (MLDi) is defined based on the anomaly of the MLD max value of the different regions. The MLDi shows a strong negative correlation in the SPE (0.53 interannual; 0.29 decadal, Table 3) on both timescales, and a strong positive anomaly in the NS (0.38 interannual, 0.57 decadal) indicating a complex, indirect and regionally different linkage. Spatial patterns of MLD show some resemblance to $\Delta pCO_2$ in the SPE with an inverse relation (Fig. 7), which can be explained by shoaling of the mixed layer leading to less ventilation of DIC rich deeper layers and thus increased $\Delta pCO_2$.

Salinity directly, but weakly influence the gas transfer (Eq. 1), but we choose to define also a SSS index (SSSi) as preliminary analysis showed a clear correlation between PP and SSS in the EC-Earth3-CC output data which can be exploited to be able to use the analysis from this study on different ESMs that might not include a biogeochemical component in possible future studies. Furthermore, the SSS dynamics also translates to the strength of the SPG, the melting of sea ice and transports of different water masses in the North Atlantic. We have defined the SSSi as the SSS anomaly in the different regions. The SSSi shows the strongest interannual correlation in the SPW (0.33), and the strongest decadal correlation in the NS (0.52) and SPW (0.39). In the composite map of the NS region, we see a strong positive SSS anomaly correlating with a positive $CO_2$ flux anomaly (Fig. 4). The SSSi shows a strong negative correlation with the $CO_2$ flux in the SPE, which is also evident in the composite maps (Fig. 7).

**Table 3**

Index analysis. Correlation coefficients are the mean of 10 ensemble members in interannual (int) and decadal (dec) timescales. In cursive min and max values for individual members are shown to indicate spread (uncertainty) of the index analysis. In bold parameters used for regression models in section 3.3.

| | Corr. Coeff. | NA Int | NA Dec | NS Int | NS Dec | NSE Int | NSE Dec | SPW Int | SPW Dec | SPE Int | SPE Dec |
|---|---|---|---|---|---|---|---|---|---|---|---|
| SPGi | mean | 0.04 | **0.31** | | | | | 0.21 | 0.44 | -0.24 | -0.17 |
| | *min* | *-0.16* | *0.08* | - | - | - | - | *-0.01* | *0.18* | *-0.42* | *-0.71* |
| | *max* | *0.16* | *0.69* | | | | | *0.25* | *0.80* | *0.05* | *0.27* |
| NSGi | mean | | | 0.30 | 0.54 | 0.25 | **0.49** | | | | |
| | *min* | - | - | *0.13* | *0.41* | *0.11* | *0.31* | - | - | - | - |
| | *max* | | | *0.53* | *0.76* | *0.40* | *0.66* | | | | |
| AMO /SSTi | mean | -0.27 | 0.19 | 0.09 | 0.36 | **-0.12** | -0.41 | **-0.25** | **0.29** | **-0.15** | **-0.38** |
| | *min* | *-0.46* | *-0.13* | *-0.05* | *0.03* | *-0.39* | *-0.64* | *-0.42* | *-0.33* | *-0.31* | *-0.83* |
| | *max* | *-0.04* | *0.56* | *0.28* | *0.59* | *0.19* | *-0.24* | *-0.12* | *0.64* | *0.03* | *0.38* |
| SICi | mean | -0.02 | -0.26 | **-0.36** | **-0.64** | | | -0.04 | -0.36 | | |
| | *min* | *-0.09* | *-0.49* | *-0.51* | *-0.84* | - | - | *-0.09* | *-0.68* | - | - |
| | *max* | *0.08* | *0.07* | *-0.17* | *-0.54* | | | *0.13* | *-0.29* | | |
| NAO | mean | 0.30 | 0.24 | 0.29 | 0.18 | 0.35 | 0.31 | 0.30 | 0.13 | 0.12 | 0.35 |
| | *min* | *0.17* | *0.02* | *0.20* | *-0.09* | *0.24* | *0.14* | *0.19* | *-0.19* | *-0.09* | *0.11* |
| | *max* | *0.46* | *0.47* | *0.37* | *0.30* | *0.44* | *0.45* | *0.46* | *0.30* | *0.32* | *0.57* |
| AMOCi | mean | **-0.40** | 0.20 | 0.11 | 0.26 | 0.17 | **-0.06** | **-0.47** | 0.16 | -0.20 | 0.02 |
| | *min* | *-0.53* | *-0.08* | *-0.06* | *0.02* | *0.05* | *-0.33* | *-0.54* | *-0.21* | *-0.33* | *-0.42* |
| | *max* | *-0.32* | *0.49* | *0.28* | *0.47* | *0.34* | *0.14* | *-0.37* | *0.42* | *-0.12* | *0.45* |
| Wi | mean | **0.68** | **0.45** | **0.73** | **0.70** | **0.72** | **0.57** | **0.80** | **0.26** | **0.24** | 0.26 |
| | *min* | *0.57* | *0.26* | *0.66* | *0.57* | *0.59* | *0.40* | *0.71* | *0.17* | *0.04* | *0.01* |
| | *max* | *0.78* | *0.56* | *0.80* | *0.83* | *0.78* | *0.66* | *0.89* | *0.80* | *0.41* | *0.43* |
| MLDi | mean | 0.02 | 0.28 | **0.38** | **0.57** | **0.33** | 0.01 | 0.14 | **0.38** | **-0.53** | **-0.29** |
| | *min* | *-0.14* | *-0.03* | *0.18* | *0.36* | *0.15* | *-0.36* | *-0.07* | *-0.12* | *-0.67* | *-0.46* |
| | *max* | *0.13* | *0.59* | *0.65* | *0.80* | *0.61* | *0.50* | *0.31* | *0.61* | *0.03* | *-0.14* |
| SSSi | mean | 0.21 | **0.31** | 0.22 | 0.52 | 0.08 | -0.24 | 0.33 | 0.39 | -0.29 | **-0.37** |
| | *min* | *-0.19* | *-0.05* | *0.02* | *0.33* | *-0.17* | *-0.49* | *0.04* | *0.03* | *-0.37* | *-0.71* |
| | *max* | *0.33* | *0.55* | *0.40* | *0.63* | *0.31* | *-0.12* | *0.45* | *0.54* | *0.03* | *0.04* |

470

### 3.3 Regression analysis

A regression model has been set up for each of the regions and both timescales, based on the findings from the composite maps and the index correlation analysis. The predictors chosen for the regression models have been chosen to provide the best possible regression model, not only focusing on the linear relationship between the predictors and the $CO_2$ flux as shown in the index analysis (Table 3). Some predictors might show a weak correlation coefficient, but contribute to a higher degree of explanation in combination with other predictors. For instance the NAO index is not considered for the regression models, as it to some degree represents the same dynamics as the wind index, and therefore does not contribute to a higher degree of explanation for the regression models. In the following, the descriptions of the regression models is based on the mean $R^2$ value of the 10 ensemble members for each region (Table 4). The regression models for the interannual variability shows slightly higher correlation/explanation for the $CO_2$ flux variability in the different regions compared to the decadal variability. In general, the NA region shows the lowest degree of correlation on both timescales, emphasising the need to divide the region into smaller regions.

The North Atlantic region interannual $CO_2$ flux can be explained by 0.48 $R^2$ by the variability in AMOC and wind speed (Table 4). The spatial patterns show a strong, homogeneous positive wind anomaly correlates well with a positive $CO_2$ flux anomaly in the NA (Fig. 3). Furthermore, the index analysis shows that both the AMOCi and Wi correlates well with the $CO_2$ flux variability (0.40 and 0.68, respectively, Table 3). The wind speed is expected to be driving the $CO_2$ flux variability, but the AMOCi represents a more dynamic control on the variability. The decadal timescale regression model includes predictors as SPGi, SSSi and Wi. Here, the $R^2$ value is 0.37 (Table 4). The composite map does not show a strong spatial pattern between the predictors and the $CO_2$ flux variability, which might explain the lower $R^2$ value. The predictors chosen for the decadal regression model align with the indexes with the greatest correlation as seen in Table 3.

The Nordic Seas region shows a good degree of explanation (0.62 and 0.58 for the interannual and decadal timescales respectively, Table 4) based on MLDi, SICi and Wi. The sea ice concentration works as a main driver for the $CO_2$ flux variability in the NS as discussed earlier and seen in Fig. 4. Furthermore, a strong positive signal in the MLD anomaly correlates with the $CO_2$ flux anomaly, indicating that dynamical processes, such as strengthening of the NSG (a deepening of the SSH) and increased convection related to disappearing sea ice also controls the $CO_2$ flux variability in the NS. The index correlation analysis also indicates the wind stress as a controlling parameter in this region in both timescales (Table 4). The fact that the regression model is based on the same parameters for both timescales indicates that the processes driving the $CO_2$ flux variability is stable across timescales for this region.

The Nordic Seas East region shows a high degree of explanation as well (0.68 and 0.53 interannual and decadal respectively, Table 4). The interannual predictors being MLDi, SSTi and Wi and the decadal NSGi, AMOCi and Wi. The interannual and decadal variability is well explained by the spatial patterns in the region (Fig. 5). However, the index analysis show a weak linear correlation between the predictors SSTi and AMOCi and the $CO_2$ flux on the interannual and decadal timescale respectively (Table 3). The low correlation coefficient in the index analysis does not however rule out, that

the SST and AMOC contribute to the variability combined with other predictors, as shown in the regression models for the

505    region. The NSE regression models show that dynamical processes such as ocean mixing and circulation drive the $CO_2$ flux

variability within the region in addition to physical parameters such as SST and wind, which is expected from the gas

transfer equations (Eq. 1-3).

The western part of the Subpolar region shows the next best degree of correlation on the interannual timescale (0.68

interannual and 0.50 decadal, Table 4). The regression model setup based on the interannual variability entails AMOCi,

510    SSTi, and Wi and show a $R^2$ value of 0.68. Based on MLDi, SSTi and Wi the regression model for the variability on decadal

timescale show a $R^2$ value of 0.50. We expected dynamic ocean processes such as the SPG strength to be controlling the $CO_2$

flux in the region, however the regression model show that the AMOCi and MLDi are predictors representing the dynamic

ocean processes. The SST anomaly shows a negative anomaly on the interannual timescale and a positive anomaly on the

decadal timescale, both correlating with a positive $CO_2$ flux anomaly (Fig. 6), which is also evident in the negative and

515    postive correlation of the SSTi in the index analysis on interannual and decadal timescale, respectively (Table 3). This shows

that the relationship between the predictors might not be linearly, and that they in combination contribute to the $CO_2$ flux

variability even though they individually do not contribute.

Lastly, the $CO_2$ flux variability in the SPE region is controlled by SST and MLD on both timescales, however, the

interannual regression model also includes Wi, and the decadal regression model includes SSSi, as indicated in Fig. 7. The

520    $R^2$ values of the regression models show that the correlation is better on the interannual timescale (0.55) than the decadal

timescale (0.40) (Table 4). Here, the regression model analysis shows that besides expected drivers such as SST and SSS (as

discussed earlier and based on Eq.1-3), dynamical processes such as ocean mixing also drives the $CO_2$ flux variability. The

MLD variability points to the SPE being a dynamical region, maybe affected by the SPG circulation in the western part of

the Subpolar region. Furthermore, SPE is an ice-free region, allowing us to understand the dynamics of the $CO_2$ flux

525    variability without the strong SIC driver. The decadal regression model for the SPE is the only one not including the Wi. The

wind speed anomaly is both negative and positive within the region, which indicates that the wind speed might not be a

controlling factor in the SPE (Fig. 7).

**Table 4**
Applied regressions for all regions across timescales. $R^2$ values based on mean $R^2$ for all ten ensemble members in interannual (int) and decadal (dec) timescales

|  | NA | | NS | | NSE | | SPW | | SPE | |
|---|---|---|---|---|---|---|---|---|---|---|
|  | Predictors | $R^2$ | Predictors | $R^2$ | Predictors | $R^2$ | Predictors | $R^2$ | Predictors | $R^2$ |
| Int | AMOCi, Wi | 0.48 | MLDi, SICi, Wi | 0.62 | MLDi, SSTi, Wi | 0.68 | AMOCi, SSTi, Wi | 0.68 | SSTi, MLDi, Wi | 0.55 |
| Dec | SPGi, SSSi, Wi | 0.37 | MLDi, SICi, Wi | 0.58 | NSGi, AMOCi, Wi | 0.53 | MLDi, SSTi, Wi | 0.50 | SSSi, MLDi, SSTi | 0.40 |

## 4. Discussion

### 4.1 Biases in ESMs

530 We calculated the $CO_2$ flux using the dependent parameters from the model as seen in Eq 1-3 to test to what degree the model $CO_2$ flux could be reproduced. Using monthly mean fields of SST, SSS, $\Delta pCO_2$ and wind speed we are able to reproduce the $CO_2$ flux variability, however to reproduce the total flux we need to use a scaled wind field (wind x 1.2). PISCES calculates the air-sea $CO_2$ flux daily (Döscher et al., 2021; Aumont et al., 2015), and by using monthly mean fields (as is the available data) we risk a smoothening of the actual daily variability that can explain the need for a scaled wind

535 field. Turner et al. (1996) discusses how using monthly mean fields for wind and temperature can affect the calculation of atmosphere–ocean fluxes (in their study dimethyl sulphide fluxes in the Nordic Seas, however using Wanninkhof (1992) gas transfer equations as in this study, Eq. 1-3). Reproducing the $CO_2$ flux helps us understand the sensitivity and dependencies on the physical parameters used to calculate the flux. The wind speed field shows a big sensitivity, which is also emphasised in the regression models, all but one entailing the Wi.

540       Earth System Models inevitably simplify the complex climate system, which will introduce biases to the modelled processes. One example being the monthly mean wind field that introduces a bias in the calculated $CO_2$ flux. Another bias addressed in this paper is the SIC bias in EC-Earth3-CC. As stated by Döscher et al., 2022; Tian et al., 2021 and shown in Fig. 1b EC-Earth3 (and thereby EC-Earth3-CC) shows an overestimation of the SIC in the Nordic Seas and the North Atlantic. The index and regression model analysis of the NS shows that the SIC is a driver of the $CO_2$ flux variability, as

545 expected based on Eq. 3. Therefore, the overestimation of sea ice extent and concentration in EC-Earth3 will undoubtebly affect and possibly control the $CO_2$ flux variability in the ocean in the EC-Earth3-CC runs. However, even in regions of sea-ice such as the SPW and the NA, SIC does not exclude significant impact of other processes, as SIC is not regarded as a predictor for the $CO_2$ flux variability in these regions (Table 3, 4).

550 ### 4.2 Predictors

Our analysis demonstrated that the $CO_2$ flux variability and its drivers cannot be assesed meaningsully considering the larger northern North Atlantic region; but instead needs to be stratified at a regional and sub-basin level. Our analysis shows a high degree of explained variability of the $CO_2$ flux within the regions defined including dynamically separated ocean regions (Table 4). Based on the regression models we have established, that a linear correlation between the $CO_2$ flux and other

555 predictors will not allow us to explain and understand the full $CO_2$ flux variability. It is clear that internal dynamics between the different predictors also affect the $CO_2$ flux variability as shown in section 3.3. Furthermore, we also establish that not only the physical parameters SST, SSS and wind speed work as drivers of the $CO_2$ flux in the regions. It is evident that wind speed poses a great control on the $CO_2$ flux variability as discussed earlier, but we also see dynamic predictors such as ocean mixing (MLDi), gyre circulation (NSGi/SPGi) and larger scale ocean circulation and transport (AMOC) as drivers. Holliday

560 et al. (2020) and Hátún et al. (2005, 2017) discuss how the larger scale dynamics such as the gyre circulation (SPG and NSG) and AMOC variability affect the SST, SSS and PP in the northern North Atlantic, aligning with our findings. Despite being the smallest region in terms of area among these studies (Table 2), the NSE region exhibits the highest variability and mean flux. This remains the case until 1960 (Fig. 2), when the SPW and NSE flux time series converge. Our regression analysis yields the highest $R^2$ values in the NSE and SPW regions (Table 4), underscoring the robustness of our approach.

565 Notably, the fact that our regression models provide the strongest explanatory power in the regions with the greatest variability and mean $CO_2$ flux suggests a stable and reliable representation of the system dynamics.

Throughout our analysis we have established that a deepening of the MLD often coincides with a positive $CO_2$ flux anomaly, which in some cases can be explained by a deepening of the MLD resulting in an increase in DIC in the surface layer, decreasing $pCO_2$ in the surface layer and thus increasing the atmosphere-ocean $CO_2$ flux (Fig 3-6). However, we also

570 see the deepening of the MLD as a response to a decrease in SIC, resulting in convection and an increase in the atmosphere–ocean $CO_2$ flux, which is especially evident in the NS region (Fig 4). The index analysis also shows a positive correlation between MLD and $CO_2$ flux in all the regions except for the SPE (Table 3). However, counter-intuitively to what is earlier established in our composite map analysis, we see a (strong) negative correlation between MLD and the $CO_2$ flux, both spatially and in the index analysis in the SPE region as mentioned (Fig. 7, Table 3). The MLDi is one of the predictors

575 defining the regression models for both timescales in the SPE, which means that the MLD variability explains a big part of the $CO_2$ flux variability, despite their counter-intuitive negative correlation. The spatial patterns of the SPE shows a negative mirroring between the $CO_2$ flux and both SSS and SST most evident on the longer timescale, but also to some degree on the short timescale (Fig. 7). Furthermore, the spatial patterns also show a possible blocking of the North Atlantic current, indicated by a closed gyre system building up SSH. The blocking of the North Atlantic current might allow for fresh, cold

580 and nutrient-rich Arctic water to enter the system, resulting in a positive $CO_2$ flux anomaly due to a decrease in temperature and nutrient supply increasing the PP and thus the $CO_2$ uptake. Increased freshwater supply from the Arctic would also result in increased stratification of the water column, indicated by the shallowing of the MLD and thereby the negative correlation between the $CO_2$ flux and MLD. We have also found that in EC-Earth3-CC, PP and SSS are more or less replaceable, including spatial patterns and their correlation. The North Atlantic is strongly influenced by the AMOC and SPG circulation, both regulating the salinity distribution and nutrient transport. The change in SSS reflects changes in the balance of

585 freshwater input (i.e. freshwater from the Arctic). Both SSS and PP are sensitive to these large scale circulation dynamics, and they might co-vary, making them somewhat interchangeable in ESMs. These observations indicate that $CO_2$ flux variability in the northern North Atlantic cannot be adequately explained by individual predictors in a linear framework. Instead, a comprehensive understanding of the underlying processes and the interactions among predictors is essential to

590 accurately capture atmosphere–ocean $CO_2$ flux variability.

## 4.3 Future projections

Based on the results of our regression model analysis we expect that the regression models are robust also for assessing the

595    $CO_2$ flux variability and tendencies in the North Atlantic from scenario simulations without a carbon cycle (EC-Earth3). This would be beneficial for estimating uncertainties related to future $CO_2$ uptake and in general to understand the carbon cycle impacts of regional climate change patterns. We have purposely defined the regression models by using non-biogeochemical predictors only. Studies have looked into the predictability of interannual-to-decadal variability: Li et al., 2016 show a predictive skill of $CO_2$ uptake in the western SPG of up to 4-7 years based on a ESM prediction system. They conclude, that

600    the predictive skill is attributed to the combination of improved ocean physical states and circulation variability, primarily in winter which corroborates our approach. Ilyina et al., 2020 shows a predictive skill for the global ocean carbon sink of up to 6 years for some EMSs. Further motivation for focussing on dynamical indices comes from Fransner et al., 2020. They show that the predictability of ocean carbon uptake correlates well with the predictability of the MLD, suggesting that the predictable signal comes from exchange of DIC with deep waters.

605         Looking into the near future, studies consistently establish that the warming of the global climate system is also manifested in warming of the ocean (Fox-Kemper et al., 2021;  Bopp et al., 2013; Fu et al., 2016; Laufkötter et al., 2016; Liu et al., 2023 Kwiatokowski et al., 2020). Ocean temperature increase would from first principles result in a decreased atmosphere–ocean $CO_2$ flux through the effects on solubility, however, as demonstrated in this study the $CO_2$ flux variability is more complex than simple linear relationships with temperature. For example,  an increased ocean temperature will lead to

610    a melting of the sea ice in the northern North Atlantic, resulting in more open ocean surface that can take up $CO_2$. However, a warming ocean will also affect the ocean circulation, both the large scale circulation and the small scale ocean mixing. AMOC is predicted to slow down with global warming (McKinley et al., 2023; Liu et al., 2023). Stagnating ocean circulation in the North Atlantic will as seen in our analysis affect the $CO_2$ flux variability in particular the SPW region of the NA, but also further north in the NSE region. Furthermore, a warming ocean combined with melting ice and stagnated

615    ocean circulation could result in increased upper ocean stratification, reduced MLD and less exchange with high DIC water masses in the deeper ocean. The predicted global warming will possibly result in stronger winds in the North Atlantic region (Lee et al., 2021, Ruosteenoja et al., 2019) which based on the gas exchange equation and our results will contribute to increasing the atmosphere–ocean $CO_2$ flux. Our results identify SIC and wind speed as main drivers of the $CO_2$ flux variability in a number of subregions of the northern North Atlantic, which would indicate an increase  in ocean $CO_2$ uptake

620    in the near future but counteracted by the direct temperature effect.

        To expand the regression analysis to investigate their robustness in scenario runs using other ESM's it is pivotal to have an in-depth understanding of the model setup and of the characteristics of indices in the specific model including biases and variability. Examples that might complicate the applicability of the regression models from this study could be how the gas transfer is handled across sea ice, how realistic the separate indices are compared to observations and how the indices

625    relate to each other. Our analysis provides a framework for identifying the key predictors and processes driving atmosphere-ocean $CO_2$ flux variability in the northern North Atlantic, but further work is necessary before applying the framework across other ESM's. We demonstrate that physical ocean and atmospheric parameters alone account for a significant portion of this variability, offering a valuable approach for assessing and understanding future $CO_2$ flux changes using readily available climate model and ocean reanalysis data.

## 5. Conclusion

Our analysis highlights the critical role of physical and dynamical processes in shaping $CO_2$ flux variability across the northern North Atlantic. Using historical simulations from the EC-Earth3-CC model, we show that key drivers, including SIC, SST, SSS, and wind stress, and ocean dynamics such as mixing and circulation, exert regionally and temporally varying influences on the atmosphere–ocean $CO_2$ fluxes. While our regression models achieve high explanatory power, they capture interannual variability more effectively than decadal trends, underscoring the dominant role of short-term fluctuations. Furthermore, our findings reveal that $CO_2$ flux variability cannot be attributed to simple linear relationships with individual predictors but instead emerges from complex interactions among multiple processes. Notably, wind stress exerts a particularly strong influence, aligning with expectations from gas transfer formulations. These results emphasize the spatially and temporally dependent nature of ocean carbon uptake and highlight the need for a multifaceted approach when assessing future $CO_2$ flux variability in a changing climate. Additionally, we conclude that the regression models we have defined in our analysis can serve as a framework for predicting and understanding future atmosphere–ocean $CO_2$ fluxes in the ESM realm. The main conclusion is that the $CO_2$ flux variability cannot be attributed to simple linear relationships with individual predictors, but instead emerges from complex interactions among multiple processes.

*Author contributions*. SMO and AP conceived and designed the study. AP wrote the majority of the manuscript, while SMO provided supervision and guidance in analysing and interpreting the results. SMO and CRL contributed to the writing and revision of the manuscript.

*Code/data availability*. EC-Earth3-CC data is available through ESGF (*https://aims2.llnl.gov/search/cmip6/*) and postprocessing scripts are available upon request.

*Competing interest*. The authors declare that they have no known competing financial interests or personal relationships that could have appeared to influence the work reported in this paper. One of the authors, CRL, serves as an Associate Editor for Biogeosciences.

*Financial support*. AP was supported by SDU's climate cluster, EU Horizon Ocean observations and indicators for climate and assessments, ObsSea4Clim, Grant agreement ID: 101136548, 10.3030/101136548 Internal contribution Nr. 15, NCKF/DMI, the Villum Foundation (grant no. 29411) and by Danmarks Fri Forskningsfond (DFF, Carolin R. Löscher, grant

660  no. 4283-00265B).

## References

Ardyna, M. and Arrigo, K.R.: Phytoplankton dynamics in a changing Arctic Ocean. *Nature Climate Change*, *10*(10), pp.892-903, https://doi.org/10.1038/s41558-020-0905-y, 2020.

665  Aumont, O., Éthé, C., Tagliabue, A., Bopp, L. and Gehlen, M.: PISCES-v2: an ocean biogeochemical model for carbon and ecosystem studies. Geoscientific Model Development Discussions, 8(2), pp.1375-1509, https://doi.org/10.5194/gmd-8-2465-2015, 2015

Berx, B. and Payne, M.R.: The Sub-Polar Gyre Index–a community data set for application in fisheries and environment research. Earth System Science Data, 9(1), pp.259-266, https://doi.org/10.5194/essd-9-259-2017, 2017

670  Bopp, L., Resplandy, L., Orr, J. C., Doney, S. C., Dunne, J. P., Gehlen, M., Halloran, P., Heinze, C., Ilyina, T., Séférian, R., Tjiputra, J., Vichi, M.: Multiple stressors of ocean ecosystems in the 21$^{st}$ century: projections with CMIP5 models. Biogeosciences. 10, 6225-6245, doi: 10.5194/bg-10-6225-2013, 2013

Boyd, P.W. and Trull, T.W.: Understanding the export of biogenic particles in oceanic waters: Is there consensus? Progress in Oceanography, 72(4), 276-312, https://doi.org/10.1016/j.pocean.2006.10.007, 2007

675  Breeden, M. L. and McKinley, G. A.: Climate impacts on multidecadal pCO 2 variability in the North Atlantic: 1948–2009, Biogeosciences, 13, 3387-3396, https://doi.org/10.5194/bg-13-3387-2016, 2016.

Broecker, W.S., Takahashi, T., Simpson, H.J. and Peng, T.H.: Fate of fossil fuel carbon dioxide and the global carbon budget. Science, 206(4417), pp.409-418, https://doi.org/10.1126/science.206.4417.409, 1979

Esbensen, S.K. and Reynolds, R.W.: Estimating monthly averaged air-sea transfers of heat and momentum using the bulk

680  aerodynamic method. Journal of physical oceanography, 11(4), pp.457-465, https://doi.org/10.1175/1520-0485(1981)011%3C0457:EMAAST%3E2.0.CO;2, 1981

Daniault, N., Mercier, H., Lherminier, P., Sarafanov, A., Falina, A., Zunino, P., Pérez, F.F., Ríos, A.F., Ferron, B., Huck, T. and Thierry, V.: The northern North Atlantic Ocean mean circulation in the early 21st century. Progress in Oceanography, 146, pp.142-158, https://doi.org/10.1016/j.pocean.2016.06.007, 2016

685  Döscher, R., Acosta, M., Alessandri, A., Anthoni, P., Arneth, A., Arsouze, T., Bergmann, T., Bernadello, R., Bousetta, S., Caron, L.P. and Carver, G.: The EC-earth3 Earth system model for the climate model intercomparison project 6. Geoscientific Model Development Discussions, 2021, pp.1-90, https://doi.org/10.5194/gmd-15-2973-2022, 2021

Friedlingstein, P., O'Sullivan, M., Jones, M.W., Andrew, R.M., Hauck, J., Landschützer, P., Le Quéré, C., Li, H., Luijkx, I.T., Olsen, A. and Peters, G.P.: Global carbon budget 2024. Earth System Science Data Discussions, 2024, pp.1-133,
690 https://doi.org/10.5194/essd-2024-519, 2024

Foukal, N.P. and Lozier, M.S.: Assessing variability in the size and strength of the N orth A tlantic subpolar gyre. Journal of Geophysical Research: Oceans, 122(8), pp.6295-6308, https://doi.org/10.1002/2017JC012798, 2017

Fox-Kemper, B., Hewitt, H.T., Xiao, C., Aðalgeirsdóttir, G., Drijfhout, S.S., Edwards, T.L., Golledge, N.R., Hemer, M., Kopp, R.E., Krinner, G., Mix, A., Notz, D., Nowicki, S., Nurhati, I.S., Ruiz, L., Sallée, J.-B., Slangen, A.B.A, Yu, Y.:
695 Ocean, Cryosphere and Sea Level Change. In Climate Change 2021: The Physical Science Basis. Contribution of Working Group I to the Sixth Assessment Report of the Intergovernmental Panel on Climate Change [Masson-Delmotte, V., P. Zhai, A. Pirani, S.L. Connors, C. Péan, S. Berger, N. Caud, Y. Chen, L. Goldfarb, M.I. Gomis, M. Huang, K. Leitzell, E. Lonnoy, J.B.R. Matthews, T.K. Maycock, T. Waterfield, O. Yelekçi, R. Yu, and B. Zhou (eds.)]. Cambridge University Press, Cambridge, United Kingdom and New York, NY, USA, pp. 1211–1362, doi:10.1017/9781009157896.011, 2021

700 Fransner, F., Counillon, F., Bethke, I., Tjiputra, J., Samuelsen, A., Nummelin, A. and Olsen, A.: Ocean biogeochemical predictions—initialization and limits of predictability. Frontiers in Marine Science, 7, p.386, https://doi.org/10.3389/fmars.2020.00386, 2020.

Fu, W., Randerson, J. T., Moore, J. K.: Climate change impacts on net primary production (NPP) and export production (EP) regulated by increasing stratification and phytoplankton community structure in CMIP5 models. Biogeosciences, 13, 5151-
705 5170, doi: 10.5194/bg-13-5151-2016, 2016.

Gruber N., Keeling, C. D., Bates, N. R.: Interannual variability in the North Atlantic Ocean carbon sink. Science, 298, 2374-2378, doi:10.1126/science.1077077, 2002.

Gregor, L. & Fay, A.: SeaFlux: harmonised sea-air CO2 fluxes from surface pCO2 data products using a standardised approach (2021.04.03) [Data set]. Zenodo, https://doi.org/10.5281/zenodo.5482547, 2021.

710 Gruber, N., Clement, D., Carter, B.R., Feely, R.A., Van Heuven, S., Hoppema, M., Ishii, M., Key, R.M., Kozyr, A., Lauvset, S.K. and Lo Monaco, C.: The oceanic sink for anthropogenic CO2 from 1994 to 2007. Science, 363(6432), pp.1193-1199, https://doi.org/10.1126/science.aau5153, 2019

Gruber, N., Bakker, D.C., DeVries, T., Gregor, L., Hauck, J., Landschützer, P., McKinley, G.A. and Müller, J.D.: Trends and variability in the ocean carbon sink. Nature Reviews Earth & Environment, 4(2), pp.119-134,
715 https://doi.org/10.1038/s43017-022-00381-x, 2023

Hátún, H., Sandø, A.B., Drange, H., Hansen, B. and Valdimarsson, H.: Influence of the Atlantic subpolar gyre on the thermohaline circulation. Science, 309(5742), pp.1841-1844, https://doi.org/10.1126/science.1114777, 2005

Hátún, H., Azetsu-Scott, K., Somavilla, R., Rey, F., Johnson, C., Mathis, M., Mikolajewicz, U., Coupel, P., Tremblay, J.É., Hartman, S. and Pacariz, S.V.: The subpolar gyre regulates silicate concentrations in the North Atlantic. Scientific
720 reports, 7(1), p.14576, https://doi.org/10.1038/s41598-017-14837-4, 2017

Häkkinen, S., Rhines, P.B. and Worthen, D.L.:. Northern North Atlantic sea surface height and ocean heat content variability. Journal of Geophysical Research: Oceans, 118(7), pp.3670-3678, https://doi.org/10.1002/jgrc.20268, 2013

Holliday, N.P., Bersch, M., Berx, B., Chafik, L., Cunningham, S., Florindo-López, C., Hátún, H., Johns, W., Josey, S.A., Larsen, K.M.H. and Mulet, S.: Ocean circulation causes the largest freshening event for 120 years in eastern subpolar North
725     Atlantic. Nature communications, 11(1), p.585, https://doi.org/10.1038/s41467-020-14474-y, 2020

Hughes, P.J., Bourassa, M.A., Rolph, J.J. and Smith, S.R.: Averaging-related biases in monthly latent heat fluxes. Journal of Atmospheric and Oceanic Technology, 29(7), pp.974-986, https://doi.org/10.1175/JTECH-D-11-00184.1, 2012

Ilyina, T., Li, H., Spring, A., Müller, W.A., Bopp, L., Chikamoto, M.O., Danabasoglu, G., Dobrynin, M., Dunne, J., Fransner, F. and Friedlingstein, P.: Predictable variations of the carbon sinks and atmospheric CO2 growth in a multi-model
730     framework. Geophysical Research Letters, 48(6), https://doi.org/10.1029/2020GL090695, 2021.

Jones, C.D., Arora, V., Friedlingstein, P., Bopp, L., Brovkin, V., Dunne, J., Graven, H., Hoffman, F., Ilyina, T., John, J.G. and Jung, M.: C4MIP–The coupled climate–carbon cycle model intercomparison project: Experimental protocol for CMIP6. Geoscientific Model Development, 9(8), pp.2853-2880, https://doi.org/10.5194/gmd-9-2853-2016, 2016

Kerr, R.A.: A North Atlantic climate pacemaker for the centuries. Science, 288(5473), pp.1984-1985,
735     https://doi.org/10.1126/science.288.5473.1984, 2000

Khatiwala, S., Primeau, F., and Hall, T.: Reconstruction of the history of anthropogenic CO2 concentrations in the ocean, Nature, 462, 346-349, https://doi.org/10.1038/nature08526, 2009

Khatiwala, S., Tanhua, T., Mikaloff Fletcher, S., Gerber, M., Doney, S.C., Graven, H.D., Gruber, N., McKinley, G.A., Murata, A., Ríos, A.F. and Sabine, C.L.: Global ocean storage of anthropogenic carbon, Biogeosciences, 10(4), pp.2169-219,
740     https://doi.org/10.5194/bg-10-2169-2013, 2013

Kwiatkowski, L., Torres, O., Bopp, L., Aumont, O., Chamberlain, M., Christian, J. R., Dunne, J. P., Gehlen, M., Ilyina, T., John, J. G., Lenton, A., Li, H., Lovenduski, N. S., Orr, J. C., Palmieri, J., Santana-Falcón, Y., Schwinger, J., Séférian, R., Stock, C. A., Tagliabue, A., Takano, Y., Tjiputra, J., Toyama, K., Tsujino, H., Watanabe, M., Yamamoto, A., Yool, A., and Ziehn, T.: Twenty-first century ocean warming, acidification, deoxygenation, and upper-ocean nutrient and primary
745     production decline from CMIP6 model projections, Biogeosciences, 17, 3439–3470, https://doi.org/10.5194/bg-17-3439-2020, 2020.

Landschützer, P., Gruber, N. and Bakker, D.C.: Decadal variations and trends of the global ocean carbon sink. Global Biogeochemical Cycles, 30(10), pp.1396-1417, https://doi.org/10.1002/2015GB005359, 2016

Laufkötter, C., Vogt, M., Gruber, N., Aumont, O., Bopp, L., Doney, S. C., Dunne, J. P., Hauck, J., John, J. G., Lima, I. D.,
750     Seferian, R., Völker, C.: Projected decreases in future marine export production: the role of the carbon flux through the upper ocean ecosystem. Biogeosciences, 13, 4023-4047, doi:10.5194/bg-13-4023-2016, 2016

Le Quéré, C., Moriarty, R., Andrew, R.M., Canadell, J.G., Sitch, S., Korsbakken, J.I., Friedlingstein, P., Peters, G.P., Andres, R.J., Boden, T.A. and Houghton, R.A.: Global carbon budget 2015. Earth System Science Data, 7(2), pp.349-396, https://doi.org/10.5194/essd-7-349-2015, 2015

755 Le Quéré, C., Andrew, R.M., Friedlingstein, P., Sitch, S., Hauck, J., Pongratz, J., Pickers, P.A., Korsbakken, J.I., Peters, G.P., Canadell, J.G. and Arneth, A.: Global carbon budget 2018. Earth System Science Data, 10(4), pp.2141-2194, https://doi.org/10.5194/essd-10-2141-2018, 2018

Lee, J.-Y., Marotzke, J., Bala, G., Cao, L., Corti, S., Dunne, J.P., Engelbrecht, F., Fischer, E., Fyfe, J.C., Jones, C., Maycock, A., Mutemi, J., Ndiaye, O., Panickal, S., Zhou, T.:Future Global Climate: Scenario-Based Projections and Near-Term

760 Information. In Climate Change 2021: The Physical Science Basis. Contribution of Working Group I to the Sixth Assessment Report of the Intergovernmental Panel on Climate Change [Masson-Delmotte, V., P. Zhai, A. Pirani, S.L. Connors, C. Péan, S. Berger, N. Caud, Y. Chen, L. Goldfarb, M.I. Gomis, M. Huang, K. Leitzell, E. Lonnoy, J.B.R. Matthews, T.K. Maycock, T. Waterfield, O. Yelekçi, R. Yu, and B. Zhou (eds.)]. Cambridge University Press, Cambridge, United Kingdom and New York, NY, USA, pp. 553–672, doi:10.1017/9781009157896.006, 2021.

765 Leseurre, C., Lo Monaco, C., Reverdin, G., Metzl, N., Fin, J., Olafsdottir, S. and Racapé, V.: Ocean carbonate system variability in the North Atlantic Subpolar surface water (1993–2017). Biogeosciences, 17(9), pp.2553-2577, https://doi.org/10.5194/bg-17-2553-2020, 2020

Li, H., Ilyina, T., Müller, W.A. and Sienz, F.: Decadal predictions of the North Atlantic CO2 uptake. Nature communications, 7(1), p.11076, https://doi.org/10.1038/ncomms11076, 2016

770 Liu, Y., Moore, J.K., Primeau, F. et al. Reduced $CO_2$ uptake and growing nutrient sequestration from slowing overturning circulation. Nat. Clim. Chang. 13, 83–90, https://doi.org/10.1038/s41558-022-01555-7, 2023

McKinley. G. A., Bennington, V., Meinshausen, M., Nicholls, Z.: Modern air-sea flux distributions reduce uncertainty in the future ocean carbon sink. Environ. Res. Lett. 18, 044011, doi:10.1088/1748-9326/acc195, 2023.

Madec, G.: NEMO ocean engine, 2015.

775 Mikaloff Fletcher, S. E., Gruber, N., Jacobson, A. R., Doney, S. C., Dutkiewicz, S., Gerber, M., Follows, M., Joos, F., Lindsay, K., Menemenlis, D., Mouchet, A., Müller, S. A., and Sarmiento, J. L.: Inverse estimates of anthropogenic CO2 uptake, transport, and storage by the ocean, Global Biogeochemical Cycles, 20, https://doi.org/10.1029/2005GB002530, 2006.

Orvik, K.A.: Long-term moored current and temperature measurements of the Atlantic inflow into the Nordic Seas in the

780 Norwegian Atlantic Current; 1995–2020. Geophysical Research Letters, 49(3), doi: https://doi.org/10.1029/2021GL096427, 2022

Polyakov, I.V., Beszczynska, A., Carmack, E.C., Dmitrenko, I.A., Fahrbach, E., Frolov, I.E., Gerdes, R., Hansen, E., Holfort, J., Ivanov, V.V. and Johnson, M.A.: One more step toward a warmer Arctic. Geophysical Research Letters, 32(17), https://doi.org/10.1029/2005GL023740, 2005

785 Ruosteenoja, K., Vihma, T. and Venäläinen, A.: Projected changes in European and North Atlantic seasonal wind climate derived from CMIP5 simulations. Journal of Climate, 32(19), pp.6467-6490, https://doi.org/10.1175/JCLI-D-19-0023.1, 2019.

Sabine, C. L., Feely, R. A., Gruber, N., Key, R. M., Lee, K., Bullister, J. L., Wanninkhof, R., Wong, C., Wallace, D. W., and Tilbrook, B.: The oceanic sink for anthropogenic CO2, science, 305, 367-371, https://doi.org/10.1126/science.1097403, 790 2004.

Sanders, R., Henson, S.A., Koski, M., Christina, L.D.L.R., Painter, S.C., Poulton, A.J., Riley, J., Salihoglu, B., Visser, A., Yool, A., Bellerby, R.: The biological carbon pump in the North Atlantic. Progress in Oceanography, 129, 200-218, https://doi.org/10.1016/j.pocean.2014.05.005, 2014.

Schulzweida, U., Müller, R., Kornblüh, L., Ansorge, C. and Quast, R.: CDO–Climate Data Operators–v2. 5.0. Center for 795 Marine and Atmospheric Sciences (ZMAW), Max-Planck Institute for Meteorology, University of Hamburg, https://code.mpimet.mpg.de/projects/cdo/embedded/index.html (last update: November 2024), 2012

Sigman, D. M. and Boyle, E.A.: Glacial/interglacial variations in atmospheric carbon dioxide. Nature, 407(6806), 859-869, https://doi.org/10.1038/35038000, 2000.

Simmonds, I. and Dix, M.: The use of mean atmospheric parameters in the calculation of modeled mean surface heat fluxes 800 over the world's oceans. Journal of physical oceanography, 19(2), pp.205-215, https://doi.org/10.1175/1520-0485(1989)019%3C0205:TUOMAP%3E2.0.CO;2, 1989

Takahashi, T., Broecker, W.S. and Langer, S.: Redfield ratio based on chemical data from isopycnal surfaces. Journal of Geophysical Research: Oceans, 90(C4), pp.6907-6924, https://doi.org/10.1029/JC090iC04p06907, 1985.

Takashi, T., Sutherland, S. C., Wanninkhof, R., Sweeney, C., Feely, R. A., Chipman, D. W., Hales, B. Friederich, G., 805 Chavez, F., and Sabine, C.: Climatological mean and decadal change in surface ocean pCO2, and net sea–air CO$_2$ flux over the global oceans. Deep Sea Research Part II: Topical Studies in Oceanography, 56, 554-577, https://doi.org/10.1016/j.dsr2.2008.12.009, 2009.

Terhaar, J., Frölicher, T.L. and Joos, F.: Observation-constrained estimates of the global ocean carbon sink from Earth system models. Biogeosciences, 19(18), pp.4431-4457, https://doi.org/10.5194/bg-19-4431-2022, 2022

810 Terhaar, J.: Drivers of decadal trends in the ocean carbon sink in the past, present, and future in Earth system models. Biogeosciences, 21(17), pp.3903-3926, https://doi.org/10.5194/bg-21-3903-2024, 2024

Thomas, M.D. and Zhang, R.: Two sources of deep decadal variability in the central Labrador Sea open-ocean convection region. Geophysical Research Letters, 49(11), p.e2022GL098825, https://doi.org/10.1029/2022GL098825, 2022

Tian, T., Yang, S., Karami, M.P., Massonnet, F., Kruschke, T. and Koenigk, T.: Benefits of sea ice initialization for the 815 interannual-to-decadal climate prediction skill in the Arctic in EC-Earth3. Geoscientific Model Development, 14(7), pp.4283-4305, https://doi.org/10.5194/gmd-14-4283-2021, 2021

Turner, S.M., Malin, G., Nightingale, P.D. and Liss, P.S.: Seasonal variation of dimethyl sulphide in the North Sea and an assessment of fluxes to the atmosphere. Marine Chemistry, 54(3-4), pp.245-262, https://doi.org/10.1016/0304-4203(96)00028-X, 1996

820 Vancoppenolle M., Bopp, L., Madec, G., Dunne, J., Ilyina, T., Halloran, P. R., Steiner, N.: Future Arctic Ocean primary productivity from CMIP5 simulations: Uncertain outcome, but consistent mechanisms. Global Biogeochemical cycles, 27, 605-619, doi:10.1002/gbc.20055, 2013

Volkov, D.L., Smith, R.H., Garcia, R.F., Smeed, D.A., Moat, B.I., Johns, W.E. and Baringer, M.O.: Florida Current transport observations reveal four decades of steady state. Nature Communications, 15(1), p.7780,

825 https://doi.org/10.1038/s41467-024-51879-5, 2024

Wanninkhof, R.: Relationship between wind speed and gas exchange over the ocean. Journal of Geophysical Research: Oceans, 97(C5), pp.7373-7382, https://doi.org/10.1029/92JC00188, 1992

Wanninkhof, R.: Relationship between wind speed and gas exchange over the ocean revisited. Limnology and Oceanography: Methods, 12(6), pp.351-362, https://doi.org/10.4319/lom.2014.12.351, 2014

830 Zou, S., Bower, A.S., Lozier, M.S. and Furey, H.H.: Deep ocean circulation in the subpolar North Atlantic observed by acoustically-tracked floats. Progress in Oceanography, 211, p.102975, https://doi.org/10.1016/j.pocean.2023.102975, 2023

Yu, J., Menviel, L., Jin, Z.D., Thornalley, D.J.R., Foster, G.L., Rohling, E.J., McCave, I.N., McManus, J.F., Dai, Y., Ren, H. and He, F.: More efficient North Atlantic carbon pump during the last glacial maximum. Nature Communications, 10(1), p.2170, https://doi.org/10.1038/s41467-019-10028-z, 2019.